

CONTENTS

I. Introduction	2
A. Rational design of gas-adsorbent materials	2
B. Computational simulation techniques for modeling of GAM	3
C. Capabilities of density functional theory methods	4
D. DFT challenges in GAM design	4
E. Inherent complexity of DFT benchmark studies	4
F. Focus and organization of this review	6
II. Nanostructured GAM	6
A. GAM desiderata	7
1. H ₂ storage	7
2. Carbon capture and sequestration	7
B. Carbon nanomaterials	9
C. Metal-organic frameworks	9
III. Density Functional Theory Methods	10
A. General considerations	10
B. Local and semi-Local E_{xc} energy functionals	10
C. Meta-GGA or highly parametrized E_{xc} energy functionals	11
D. Hybrid exchange energy functionals	11
E. Dispersion-corrected E_{xc} energy functionals	12
F. The random phase approximation and DFT+MBD	12
IV. Assessing the performance of DFT methods in the design of GAM	14
A. H ₂ storage	14
1. Carbon-based GAM	14
2. MOF	18
B. CO ₂ capture and sequestration	19
1. Carbon-based GAM	19
2. MOF	21
V. Discussion and Prospective Work	24
VI. General Conclusions	26
Acknowledgments	27
References	27

The Role of Density Functional Theory Methods in the Prediction of Nanostructured Gas-Adsorbent Materials

Claudio Cazorla*

*School of Materials Science and Engineering, University of New South Wales, Sydney NSW 2052, Australia
Integrated Materials Design Centre, University of New South Wales, Sydney NSW 2052, Australia*

With the advent of new synthesis and large-scale production technologies, nanostructured gas-adsorbent materials (GAM) such as carbon nanocomposites and metal-organic frameworks are becoming increasingly more influential in our everyday lives. First-principles methods based on density functional theory (DFT) have been pivotal in establishing the rational design of GAM, a factor which has tremendously boosted their development. However, DFT methods are not perfect and due to the stringent accuracy thresholds demanded in modeling of GAM (e.g., exact binding energies to within ~ 0.01 eV) these techniques may provide erroneous conclusions in some challenging situations. Examples of problematic circumstances include gas-adsorption processes in which both electronic long-range exchange and nonlocal correlations are important, and systems where many-body energy and Coulomb screening effects cannot be disregarded. In this critical review, we analyze recent efforts done in the assessment of the performance of DFT methods in the prediction and understanding of GAM. Our inquiry is constrained to the areas of hydrogen storage and carbon capture and sequestration, for which we expose a number of unresolved modeling controversies and define a set of best practice principles. Also, we identify the subtle problems found in the generalization of DFT benchmark conclusions obtained in model cluster systems to real extended materials, and discuss effective approaches to circumvent them. The increasing awareness of the strengths and imperfections of DFT methods in the simulation of gas-adsorption phenomena should lead in the medium term to more precise, and hence even more fruitful, *ab initio* engineering of GAM.

PACS numbers: 31.15.-p, 71.15.Mb, 81.05.Zx, 81.05.U-, 81.05.Rm

I. INTRODUCTION

A. Rational design of gas-adsorbent materials

Nanostructured gas-adsorbent materials (GAM) are the cornerstones of potentially revolutionary advancements in critical and fast growing technological fields like molecular sensing, energy storage and harvesting, and environmental and sustainability engineering. Their exceptional high surface to volume ratio, regular atomic composition, tunable reactivity, transport properties, and assembling affinity to form supramolecular systems, have permitted the realization of timely and cost-effective applications like, for instance, the detection and removal of toxic substances from water and air, dense storage of hydrogen and natural gas in solid state matrices, sequestration of carbon dioxide from flue gases generated in electricity production plants, design of high-performance photovoltaic cells, and enhanced long-lasting operation of batteries, to cite just a few examples [1–5].

Popular families of nanostructured GAM include zeolites, metal oxides nanocrystals (e.g., CaO and Al₂O₃), carbon-based nanomaterials (CN, e.g., nanotubes, sheets, met-cars, graphite intercalation compounds, and frameworks of organic pillared graphene), metal hydrides nanoparticles (e.g., MgH₂ and LiBH₄), and covalent- and metal-organic frameworks (COF and

MOF). Of all these species CN and MOF (see Fig. 1) stand out as some of the most promising GAM for energy and environmental applications, particularly to what concerns the capture and storage of hydrogen (H₂), carbon dioxide (CO₂), and methane gases [6–15].

Currently reported GAM gas-selectivity and storage capacities, however, still remain below the stringent commercial targets set by specialized government bodies and agencies. For instance, hydrogen storage systems need to achieve an overall capacity of 5.5 wt% hydrogen with a volumetric ratio of 40 g/L for competitive vehicle applications [16], and capture of the 90 % of the carbon dioxide produced in the generation of electricity must be reached within less than a 35 % of increase in the final costs [17, 18]. The search for optimal gas-adsorption processes and GAM, therefore, remains an area of very active scientific and technological research.

A key aspect for potential GAM to be successful is to find the optimal chemical compositions and pore topologies to work under specific thermodynamic conditions. The number of possible stoichiometric and structural GAM configurations is tremendously large, hence in practice systematic experimental searches based on trial-error strategies turn out to be cumbersome and very inefficient. Rational engineering of gas-adsorbent interactions at the atomic scale, represents a key notion to achieve success on such a design grand challenge in the short and middle term. In this context, computational simulation methods emerge as invaluable theoretical tools for the screening and rational engineering of auspicious GAM.

* c.cazorla@unsw.edu.au

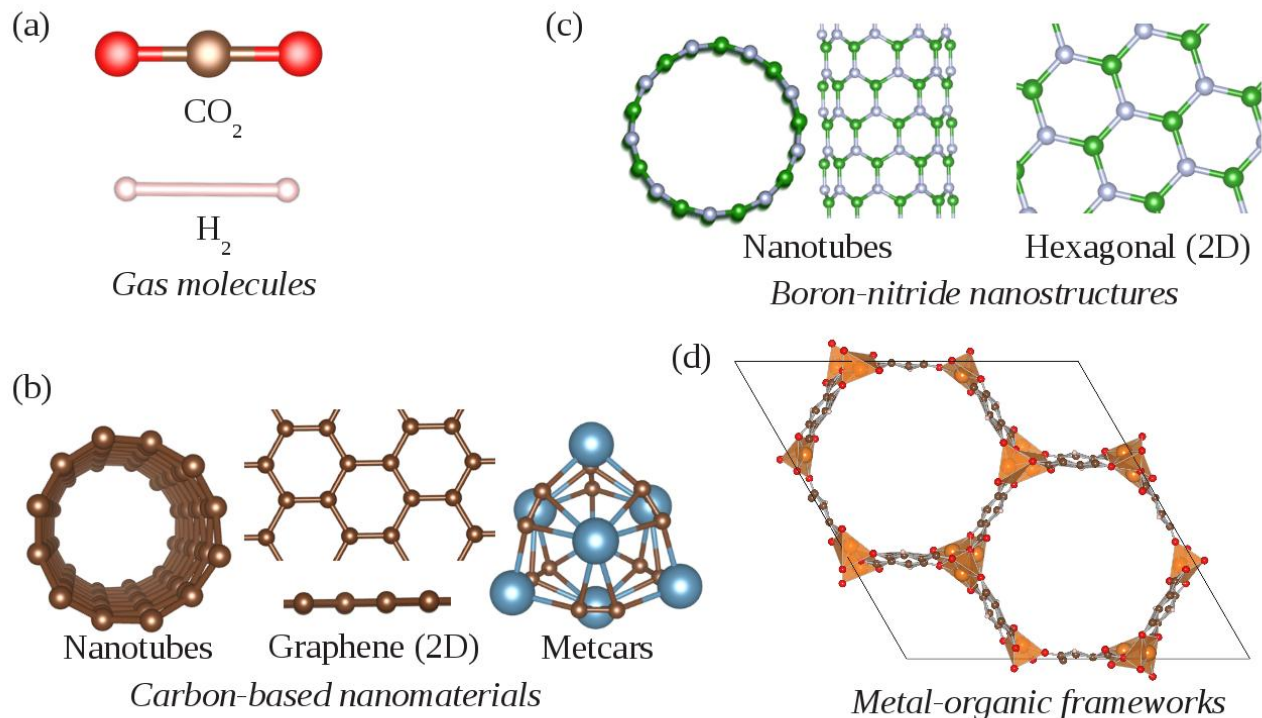


FIG. 1. (a) Representation of the gas species considered in this review and (b)-(d) some of the most popular families of nanostructured gas-adsorbent materials: carbon-based nanomaterials, boron-nitride nanostructures and MOF (see text).

B. Computational simulation techniques for modeling of GAM

Common simulation techniques in the study of GAM can be classified into two major categories: “semi-empirical” and “first-principles”. In semi-empirical approaches, the interactions between atoms are modeled with analytical functions, known as force fields or classical potentials, which are devised to reproduce a certain amount of experimental data or the results of high-accuracy calculations. The inherent simplicity of classical potentials makes it possible to address the study of GAM and gas-adsorption processes considering realistic thermodynamic conditions and length/time scales, with well-established simulation techniques like, for instance, molecular dynamics and grand canonical Monte Carlo [19]. With the current computational power and algorithm development, key features in GAM which are directly comparable to observations (e.g., adsorption isotherms, elastic properties and diffusion coefficients [20–24]) can be computed routinely on a standard office computer. Also, the relevance of quantum nuclear effects in gas-adsorption phenomena can be estimated accurately with semi-empirical approaches [25–28]. Nevertheless, in spite of the great versatility of semi-empirical methods, classical potentials may present impeding transferability issues in certain situations. This type of drawbacks is related to the impossibility of mim-

icking the features of the targeted material at conditions different from those in which the setup of the corresponding force field was performed [29, 30].

In this context, the outputs of first-principles calculations turn out to be crucial. As the name indicates, empirical information is not contained on first-principles methods, also known as *ab initio*. The interactions between atoms are directly obtained from applying the principles of quantum mechanics to the electrons and nuclei. Transferability issues, therefore, are totally missing in *ab initio* approaches. Examples of first-principles techniques include, density functional theory and quantum Monte Carlo, to cite just a few. Although these approaches are very accurate, they can be also very demanding in terms of computational expense. This circumstance poses serious difficulties to the study of kinetic and thermodynamic effects in extended GAM with *ab initio* techniques. Common acceleration schemes within first-principles methods entail the use of pseudopotentials [31, 32]. Many materials properties can be predicted basing exclusively on the behaviour of the valence electrons, and by employing pseudopotential techniques explicit treatment of the core electrons is avoided in the simulations. Pseudopotentials can actually be the source of potential errors, however they make also the simulation of heavy atoms and medium-size systems feasible. Fortunately, some strategies can be used to minimize the impact of the approximations introduced by pseudopen-

tials like, for instance, the projector augmented wave [33] and linearized augmented plane wave methods [34]. In the present critical review, we will concentrate on analyzing specific aspects of the simulation of GAM with first-principles methods, obviating the outcomes of indispensable and physically insightful semi-empirical approaches.

C. Capabilities of density functional theory methods

Standard density functional theory (DFT) techniques (i.e., based on local and semilocal approximations to the electronic exchange-correlation energy, typically LDA and GGA) have become the *ab initio* methods of choice in the study and design of nanostructured GAM. These techniques have been demonstrated to reproduce with notable accuracy the interplay of a wide range of interactions in hundreds-of-atoms systems, while keeping within reasonably affordable limits the accompanying computational expense. However, standard DFT methods present some well-known limitations in describing gas-adsorption phenomena occurring in low-coordinated atomic environments (e.g., the binding of small molecules to surfaces and cavities). For instance, due to the local nature of the employed energy functionals standard DFT methods cannot reproduce the electronic long-range correlations resulting from instantaneously induced dipole-dipole, dipole-quadrupole, quadrupole-quadrupole and so on interactions. Another common DFT fault is the presence of electronic self-interaction errors, which derive from an imperfect cancellation between the auto-correlation (i.e., spurious interaction of an electron with itself) and exchange energies. This type of errors can alter dramatically the description of charge-transfer complexes, chemical reactions, and electron affinities [35–38]. Fortunately, many developments have been realized during the last two decades which have solved part of these drawbacks (e.g., nonlocal and hybrid exchange-correlation energy functionals, see next section), permitting so to achieve remarkable agreement between theory and experiments. Nevertheless, a number of critical aspects remain yet challenging to customary DFT methods that could be hindering the rational design of GAM.

D. DFT challenges in GAM design

One of such challenges consists in accounting for the long-range electronic correlations while simultaneously amending the electronic self-interaction errors (see Fig. 2a). Along with the adsorption of gas molecules on surfaces, regions of significant electron depletion and accumulation may appear which induce strong electrostatic interactions and the shift of electronic energy levels. In those conditions, one could expect that by adding a portion of the exact Hartree-Fock exchange energy to

the selected DFT functional, in order to lower the electron self-interaction errors to negligible levels, accurate binding energies will follow. Reported evidence, however, suggests that accounting for weak dispersion interactions in charge-transfer processes may turn out to be also decisive [39, 40]. Unfortunately the causes behind such an unexpected result are not yet totally understood, due in part to the difficulties encountered in the decomposition of DFT energies into fundamental portions. Rationalization of this complexity clearly is needed for optimizing the computational load associated to DFT modeling of GAM (i.e., accounting for dispersion interactions normally requires intensive calculations), and also for ensuring the reliability of prospective and already published simulation works on the storage and sequestration of gases.

Another important DFT threat consists in accounting adequately for the screening of bare interactions in periodically extended systems (see Fig. 2b). Many-body energy and Coulomb screening effects can be equally important in physisorption and chemisorption phenomena, and the issues encountered in their description are a consequence of the pairwise additivity assumed in the construction of most DFT functionals. Essentially, the interaction energy between two atoms remains unaltered no matter what medium separates them or what collective excitations happen in the material [41–43]. In this context, the adiabatic connection fluctuation-dissipation (ACFD) theorem has been exploited to calculate correlation DFT energies that incorporate many-body higher-order terms. This is the case of the random phase approximation to DFT (RPA-DFT) [44–46] and the DFT+MBD [47–50] methods (see Sec. III), which at present are receiving the highest attention. Nonetheless, the development of many-body DFT-based methods are still on their infancy and the associated computational expenses are elevated (typically ranging from two to four orders of magnitude larger than standard DFT). The corresponding degree of applicability therefore remains still limited.

E. Inherent complexity of DFT benchmark studies

Most of *ab initio* works published to date on the design of GAM are based on standard DFT calculations (see Sec. V for more details). Standard DFT methods are very effective in dealing with large atomic systems and a myriad of user-friendly DFT packages, practically available to everyone nowadays, have facilitated their widespread use. However, chemical accuracy is generally demanded on GAM design (e.g., correct binding energies to within ~ 0.01 eV) and thus, for the reasons highlighted in the previous section, employing standard DFT methods may not always be adequate.

In fact, to carry out DFT benchmark tests on the assessment of GAM is of paramount importance for rigorously establishing acceptable balances between compu-

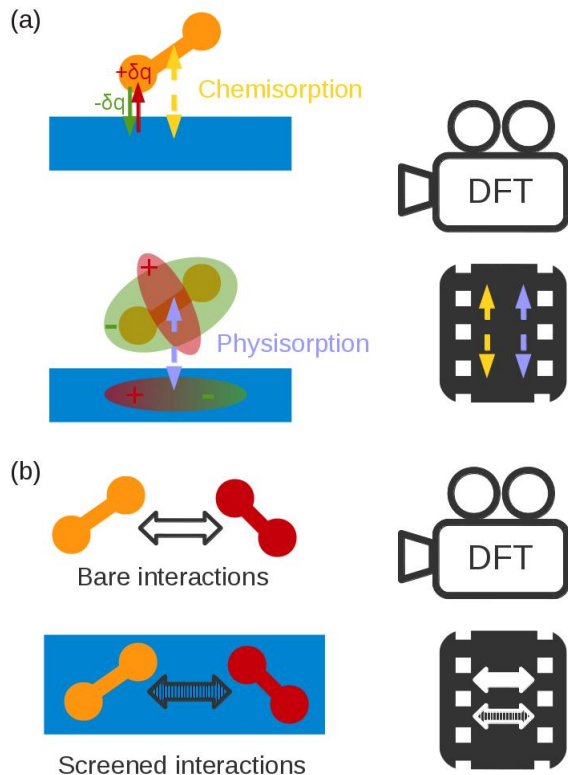


FIG. 2. Schematic representation of the two main challenges of customary DFT methods in GAM design: (a) reproduction of covalent and dispersion interactions on an equal footing and (b) description of Coulomb screening and many-body energy interactions in extended systems.

tational feasibility and predictive reliability. Performing computational studies of such a type, however, is not a trivial task. First, one has to be familiar with the technical and foundational aspects of highly accurate quantum chemistry methods (QCM) like Møller-Plesset perturbation theory (MP2), the coupled-cluster method with single, double and perturbative triple excitations [CCSD(T)], and quantum Monte Carlo (QMC), to cite just a few. In those approaches the Schrödinger equation of the many-electron system of interest is solved directly by handling the corresponding wavefunction. Many-electron wavefunctions generally are expressed in real space as a linear combination of atomic orbitals (LCAO). LCAO do not fulfill the conditions of Bloch functions and thus the simulation of periodic systems like crystals and surfaces, although possible, it is not straightforward with them [51–54]. Consequently, most QCM studies are performed in supercells containing model cluster systems where periodic boundary conditions are not applied. Meanwhile, QCM are inherently complex and the associated computational load in general scales poorly with the number of electrons (namely as N^{4-7}).

Besides the technical intricacies, a conceptual problem also arises when performing benchmark studies in model

cluster systems: on what grounds is correct to generalize the so-obtained conclusions to realistic extended materials? To help in answering this question, we show in Fig. 3 the partial density of electronic states (pDOS) calculated in graphene, i.e., an extended one-atom thick carbon surface, decorated with Ca impurities, and a coronene molecule doped with a Ca adatom (i.e., $\text{Ca@C}_{24}\text{H}_{12}$) using standard DFT methods (in both systems the ratio of Ca impurities to carbon atoms is the same). We note that the coronene molecule is generally considered as a large enough system in which to carry out computational accuracy tests. However, as it can be appreciated in the figure the pDOS computed in coronene differs greatly from the one obtained in the “equivalent” graphene-based system (e.g., compare the distribution of electronic d states around the Fermi energy level in the two cases). Also, charge-transfer calculations based on Bader’s theory show that the Ca adatom donates about $0.08 e^-$ to the coronene molecule (i.e., weak ionic interaction), whereas in Ca-decorated graphene it supplies $\sim 0.9 e^-$ to the carbon surface (i.e., strong ionic interaction). In fact, quantum confinement effects can introduce important differences in the electronic structure of apparently similar extended and cluster systems, thereby leading to completely unlike gas-adsorption behaviours in the two situations [55, 56]. In addition to this, long-range electronic exchange and nonlocal correlations, which are ubiquitous in gas-adsorption phenomena, normally turn out to be disguised in model cluster systems.

An obvious solution to overcome these likely scaling problems, affecting most benchmark studies, consists in using highly accurate quantum chemistry approaches which, alike to DFT, can handle the simulation of periodic systems. All the necessary benchmark and DFT calculations therefore can be undertaken in a same extended simulation cell. In this regard, quantum Monte Carlo (QMC) emerges as one of the most promising family of methods for benchmarking DFT. Actually, the formalism of many-electron Bloch functions has been established within QMC since long time ago [57, 58] and several implementations of this approach are already available in open-source packages like, for instance, CASINO [59], QWALK [60], and QMCPACK [61]. Also, the balance between accuracy and scalability in QMC is among the highest of all quantum chemistry methods (e.g., the accompanying computational cost climbs as N^{2-3} with the number of electrons [62]). It is worth mentioning that very recent methodological advances have permitted also the implementation of the MP2 and the CCSD approaches in a planewave framework [63–65]. The availability of this last suite of quantum chemistry techniques however is rather limited at the moment, although it is likely to improve over the next few years [66].

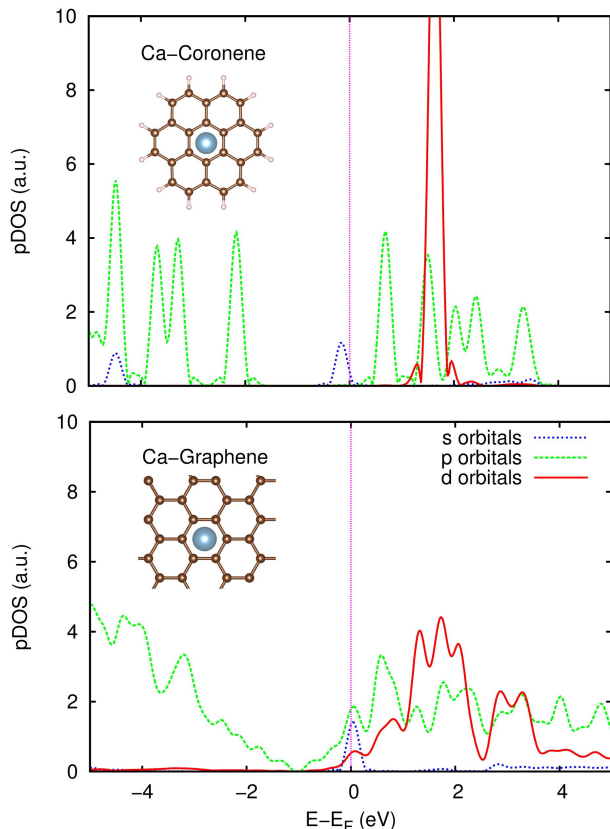


FIG. 3. Partial density of s , p , and d electronic states calculated in a $\text{Ca-C}_{24}\text{H}_{12}$ molecule (*Top*), and in Ca-doped graphene (*Bottom*). The ratio of calcium to carbon atoms is the same in both systems, namely $1/24$. Calculations have been performed with standard DFT methods, and the Fermi energy level in both systems has been shifted to zero. (This figure has been adapted from work. [138].)

F. Focus and organization of this review

The focus of the present critical review is on the assessment of the accuracy of DFT methods in the prediction and understanding of nanostructured GAM. Despite that the number of DFT studies published so far on GAM applications is enormous, there is not yet a well-established set of best practice principles for meaningful simulation of gas-adsorption phenomena and materials. The main objective of this review is to assist in defining this, by critically discussing key contributions and unsolved controversies in the field. Also, we identify here the subtle problems found in the interpretation of complex benchmark studies and propose likely solutions for them.

Our analysis is constrained to the design of carbon-based nanomaterials (CN) and MOF for applications in H_2 storage and CO_2 sequestration and capture. The main reason justifying this choice is that these types of GAM and problems currently are attracting the highest attention within the community of computational and en-

vironmental materials scientists [6–13, 67–69]. Moreover, by understanding the processes involved in the adsorption of H_2 and CO_2 molecules on CN and MOF we may infer also those affecting many other substances and materials. For instance, under normal conditions H_2 and CO_2 molecules are both linear and consequently cannot sustain any permanent dipole moment (e.g., like N_2); the predominant electrostatic interactions with the solid sorbent then are of hydrogen bond and quadrupolar type, respectively. However, when CO_2 molecules receive or donate electrons they normally get distorted and become polar. Thereby, from an electrostatic point of view CO_2 can turn out to be similar to other important molecules like, for instance, water and ammonia. On the other hand, CN and MOF are structurally and electronically alike to boron-nitride nanostructures and covalent organic frameworks (see Fig. 1), two families of GAM which at present are being investigated also very thoroughly [70–74]. For the sake of focus, other important mechanisms exploited in gas storage and sequestration processes (e.g., gas binding in bulk chemical form and thermodynamic destabilization of nanocrystals and clusters [75–79]) and related families of materials (e.g., metal oxides and binary and ternary hydride compounds [80–85]), will not be discussed exhaustively in the present work.

The organization of this review is as follows. In the next section we briefly summarize the binding energy targets pursued in the design of H_2 storage and CO_2 capture and sequestration GAM, together with a short description of CN and MOF. Next, we explain the generalities of DFT methods and provide essential insight into its most popular versions. In Sec. IV, we review the most recent and relevant works done in the assessment of the performance of DFT methods in GAM modeling. From them, we draw general conclusions on which DFT exchange-correlation functionals can be employed *safely* for the simulation of gas-adsorption processes and materials. Also, we comment on the subtle problems found in the generalization of benchmark conclusions obtained in model cluster systems to real GAM, and discuss possible solutions for them. In Sec. V, we present a discussion on the current tendencies followed in first-principles design of GAM and propose a number of new directions to explore in prospective modeling and benchmark studies. Finally, our main conclusions are outlined in Sec. VI.

II. NANOSTRUCTURED GAM

Nanostructured gas-adsorbent materials contain characteristic nanoscale motifs which are periodically repeated along one, two or three directions. Those motifs generally are composed of light atoms which congregate to form atomically sparse complexes. There are excellent review articles in the literature focusing on the physical properties and prospective implementations of GAM (see for instance Refs. [86–93]), hence we highlight here only the main traits of some representative species (i.e., CN

and MOF). Also, we explain the basic requirements that potential GAM must accomplish for achieving effective storage and sequestration of H_2 and CO_2 gases.

A. GAM desiderata

The “hydrogen storage” and “carbon dioxide capture and sequestration” problems have sparked very intense research within the communities of chemists, physicists and engineers in the last past decade. The discovery of new materials with large gas uptake capacities, robust thermodynamic stability, fast adsorption-desorption kinetics, and affordable production costs, is a key notion to succeed in the encountered gas storage and sequestration challenges [94–98].

The binding affinities of potential GAM are determined by their interactions with the gas molecules, which can be of electrostatic, dispersion, and/or orbital types [99]. In turn, the strength of the gas-GAM interactions depend on the characteristics of the materials and gas species, which in the latter case include electronic structure, atomic shape, polarizability and permanent dipole and/or quadrupole moments. Key quantities in the assessment of gas-adsorbent materials include the alignment between frontier molecular orbitals (i.e., the energy difference between the highest occupied molecular orbital -HOMO- in the adsorbate and the lowest unoccupied molecular orbital -LUMO- in the adsorbent), and the resulting charge transfers and binding energies. Let us have a closer look into the most relevant physical aspects of promising hydrogen and carbon capture GAM.

1. H_2 storage

For hydrogen to become the fuel of choice in future environmentally clean vehicles and electricity production plants, large amounts of H_2 need to be stored within relatively small volumes entailing moderate weights (for a detailed list of related targets see Refs. [100, 101]). In this context, H_2 adsorption on light solid sorbents through weak and mild molecule-GAM interactions emerges as one of the most promising routes. (Dissociative adsorption in solid metal hydrides where molecular hydrogen is dissociated to form a solid solution with the hydride, is also considered as propitious [75, 76]; however, we will not discuss such an interesting gas-storage mechanism or related family of materials in the present review for the sake of focus.) Current estimations of the optimal binding energy for adsorption of hydrogen at ambient temperature and considering safe delivery pressure conditions of 1.5 – 30 bar, amount to ~ 0.2 eV/molecule [102–104]. Meanwhile, kinetic effects may be critical for practical applications (e.g., complete H_2 storage-release cycles must be realized within seconds) and when these are taken into account favourable binding energies turn out to be ~ 0.7 eV/molecule [105]. Based on these assessments, the

binding energy range that typically is targeted in most *ab initio* H_2 -storage works is 0.1 – 1.0 eV/ H_2 , which spans from dispersion to moderately covalent molecule-GAM interactions (see Table I).

The strength of the H_2 -solid sorbent interactions can be tuned by decorating the GAM surfaces with transition or alkaline-earth metal atoms, and this normally tends to increase the affinity towards gas binding [106–108]. The orbital mechanism acting behind this effect is the Kubas interaction, which consists in electron donation from the H_2 σ -bonding orbital to the empty metal d orbitals and simultaneous electron back-donation from the filled metal d orbitals to the H_2 σ -antibonding orbital [109, 110]. A different approach that is promising for gas storage at elevated temperatures, is the spillover of hydrogen onto inert surfaces. This mechanism implies the chemical activation of H_2 molecules placed on top of transition metal sites through catalysis, followed by the migration of atomic hydrogen onto the surface of the receptor material (e.g., activated carbons, COF, and MOF). Record hydrogen storage capacities of 4 – 6 wt. % have been recently accomplished with this strategy in metal-carbon complexes and MOF [111–115].

2. Carbon capture and sequestration

Carbon capture and sequestration (CCS) actions are being implemented in fossil-fuel burning power plants for cutting the amounts of green-house gases which are expelled to the atmosphere. Current CCS means mostly rely on the scrubbing of synthesis and flue gases with amine solvents. However, solvent-based CCS technologies generally are not cost-effective due to the high energy penalty involved in solvent regeneration and equipment corrosion [116]. Fortunately, membranes and solid sorbents do not suffer from these important drawbacks and thus they constitute the core of next-generation CCS technologies.

There are two main types of CCS processes in which GAM are highly promising: pre-combustion and post-combustion. In pre-combustion CCS, the fuel is converted into a mixture of hydrogen and carbon dioxide gases using processes such as “gasification” or “reforming”. The usual thermodynamic conditions in pre-combustion CCS are high temperatures and high pressures (i.e., above 100° and 20 – 30 bar, respectively), and the concentration of CO_2 gas is high. At those conditions, it can be shown that CO_2 sequestration turns out to be effective when the strength of the gas-GAM interactions roughly amounts to 2.0 eV/molecule. For this, consider the inverse calcination reaction, $CaO + CO_2 \rightarrow CaCO_3$, to be a model of a typical pre-combustion CCS process [77–79]. The Gibbs free-energy balance of this reaction has been approximated by the function $\Delta G = -1.83 + 0.0016 \cdot T$ eV/molecule, where T represents the temperature (expressed in Kelvin) [117]. Now, by assuming that the thermal contributions to ΔG mostly arise

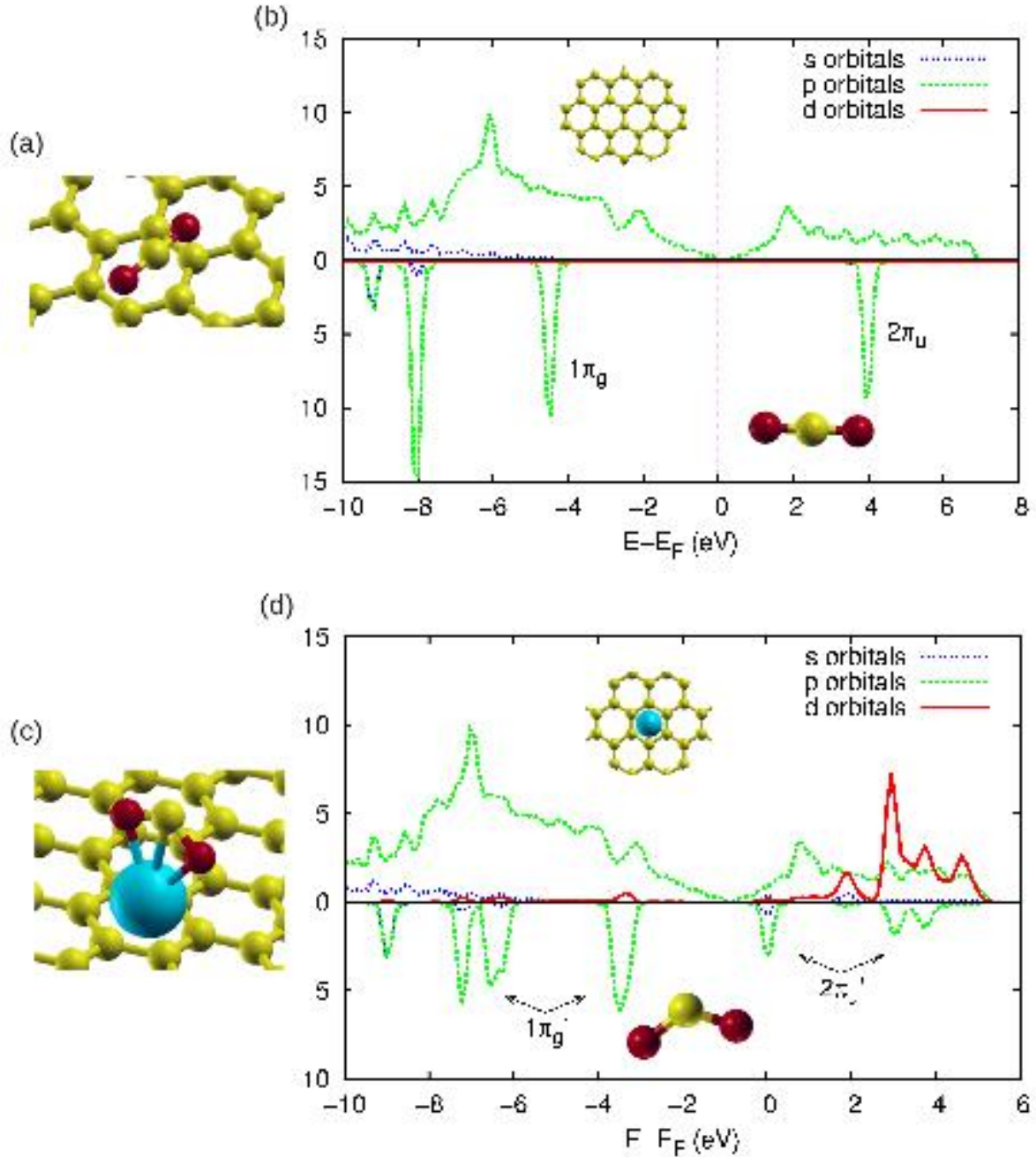


FIG. 4. (a) Sketch of a carbon dioxide molecule interacting with a carbon-based surface. (b) Partial density of electronic states calculated in the system sketched in (a), expressed in arbitrary units. The electronic states localized in the carbon surface are represented in the upper part of the figure, and those corresponding to the gas molecule in the lower. (c) Sketch of a carbon dioxide molecule interacting with a Ca-decorated carbon surface. (d) Partial density of electronic states calculated in the system sketched in (c), expressed in arbitrary units. The electronic states localized in the Ca-decorated carbon surface are represented in the upper part of the figure and those corresponding to the gas molecule in the lower. HOMO bonding and LUMO anti-bonding molecular orbitals are indicated in panels (b) and (d) [see text].

from the entropy of the gas, $E_{\text{bind}} \sim 2.0$ eV/molecule follows.

In post-combustion CCS, the CO_2 gas is separated from the exhaust of a combustion process. The usual thermodynamic conditions in post-combustion CCS are

low temperatures and low partial CO_2 pressures. In that case, it can be shown that the ideal gas-binding energy scale for solid sorbents is ~ 0.2 eV/molecule. For this, consider that a typical CCS post-combustion process can be described by the generic capture reac-

tion $A + n\text{CO}_2 \rightarrow A(\text{CO}_2)_n$, and that the corresponding Gibbs free-energy balance vanishes at temperatures close to ambient (e.g., 50° degrees Celsius). Now, by assuming that the entropy change in the solid sorbent A upon adsorption of molecules is practically null and using tabulated thermodynamic data of the CO_2 gas (i.e., the corresponding entropy is $S_{\text{gas}} = 5.3 \cdot 10^{-4}$ eV/molecule K), $E_{\text{bind}} \sim 0.2$ eV/molecule follows.

Based on these assessments, typical gas-adsorption energies pursued in most *ab initio* CCS studies span from 0.2 to 2.0 eV/ CO_2 , and depending on the specific aims one end or the other of this interval is targeted. As it is shown in Table I, that energy range extends from weak dispersion to strong covalent molecule-GAM interactions. In addition to these binding energy requirements, prospective CCS GAM need to display also favorable selectivity features with respect to the adsorption of N_2 , oxygen and water, since those species are also abundant in the generated flue and synthesis gases.

It is worth mentioning that similar electronic orbital processes to the Kubas interaction [109, 110] explained in the previous section, can be exploited also for enhancing the affinities of GAM towards CO_2 binding. In Fig. 4, we represent the partial density of electronic states calculated for a carbon dioxide molecule interacting with a pristine carbon surface, and with the same surface decorated with Ca atoms. The presence of calcium dopants induces overlappings between electronic p CO_2 orbitals and s, d metallic states in the region surrounding the Fermi level, resulting in a transfer of charge from the molecule to the metal centers. In this process the degeneracy of the HOMO $1\pi_g$ bonding and LUMO $2\pi_u$ antibonding molecular orbitals is lifted, and electronic charge is back-donated from the filled s, d Ca orbitals to the antibonding CO_2 electronic states (compare bottom panels in both Figs. 3 and 4). This orbital mechanism provokes the bending of the gas molecule and intensifies the gas-GAM interactions [118], thus providing a route for the rational design of sorbent materials for pre-combustion CCS applications.

B. Carbon nanomaterials

Carbon nanostructures (CN) include an ample range of carbon allotropes such as nanotubes, graphene, met-cars and graphite intercalation compounds (see Fig. 1). CN exhibit a large variety of electronic and transport properties resulting from the specific way in which atoms are arranged. Carbon nanotubes, for instance, may be metallic or semiconducting depending on their diameter and the degree of helicity present in their hexagonal-ring walls [119, 120]. Met-cars (i.e., metallocarbohedrynes) are extremely stable symmetric clusters formed by metal and carbon atoms with stoichiometric formula M_nC_m , where M typically stands for a transition metal atom ($M = \text{Ti}, \text{V}, \text{Zr}, \text{Hf}, \text{Fe}, \text{Cr}, \text{and Mo}$) and $n, m = 8, 12$ (see Fig. 1) [121, 122]. Graphite intercalation compounds

(not shown in Fig. 1) are composed of alternating planes of transition, alkali or alkaline-earth metal and C atoms disposed in triangular and hexagonal lattices, respectively. In these materials relative shifts between successive atomic planes along the out-of-plane direction may occur leading to the formation of stacking patterns [123–125].

Interestingly, the electronic and gas-adsorption properties of CN can be finely tuned by coating their surfaces with dopant species, creating defects, or imposing mechanical strains [126–131]. Among these, the doping strategy with metal adatoms has attracted a lot of attention because of its technical simplicity and expected enhancement of the binding affinity towards gas molecules through the Kubas interaction [109, 110] (see Sec. II A 1) [132–135]. However, transition metal atoms in carbon surfaces exhibit a strong tendency towards clustering [136–138] and thereby further developments in the field of synthetic chemistry addressing this problem are awaited. Alternatively, the creation of nanostructured networks of defect sites such as vacancies, nanoribbons and islands, may increase considerably the number of unsaturated carbon sites. This kind of structural modifications generally enhance the interactions with the gas molecules and therefore lead to improved gas storage capacities [139, 140].

C. Metal-organic frameworks

Metal-organic frameworks (MOF) are multi-dimensional nanoporous structures composed of metal ions (or clusters) coordinated to rigid organic molecules, which are called linkers. The choice of the metal ion and linker species completely determines the structure and functionality of the resulting MOF. Common organic linkers include bidentate carboxylics (e.g., HOOC-COOH), tridentate carboxylates (e.g., $\text{C}_9\text{H}_6\text{O}_6$), 1,4-benzenedicarboxylate (BDC), and azoles (e.g., $\text{C}_2\text{H}_3\text{N}_3$) molecules. The great freedom with which the linkers and metal ions can be chosen and combined is reflected in the more than 20,000 MOF species that have been reported in the last two decades (for an extensive review on this topic, see Ref. [141]). Among these, the A-MOF74 ($A = \text{Mg}$ and Ni), MOF-5 (e.g., Zn_4O tetrahedra linked by BDC organic molecules) and X-BTT ($X = \text{Ca}, \text{Fe}, \text{Mn}, \text{Cu}, \text{Co}, \text{Ni}, \text{Cr}, \text{and Cd}$, and $\text{BTT} = 1, 2, 5\text{-benzenetristetrazolate}$) families emerge as three of the most investigated compounds. The A-MOF74 structure is based on coordinated carboxyl and hydroxy groups (i.e., helical A-O-C rods that emanate from 6-coordinated A centers) and its primitive unit cell contains 54 atoms. The MOF-5 crystal has a cubic symmetry and its conventional and primitive cell contain eight and four $\text{OZn}_4\text{O(BDC)}_3$ formula units, respectively (i.e., 424 and 106 atoms). The primary building block of X-BTT is a truncated octahedron (i.e., a six $[\text{X}_4\text{Cl}]^{+7}$ squares and eight BTT ligands structure)

which shares its square faces to form a general cubic framework, comprising a total of 210 atoms.

The polarity of the building units and spatial separation between the organic linkers, affect profoundly the binding strength of H_2 and CO_2 molecules and thereby constitutes a rationale for the design of MOF-based GAM. Also, decorating the MOF surfaces with alkali, alkaline-earth and transition metal atoms can enhance significantly the adsorption of gas species. Practical realizations of this last type of functionalization, however, remain yet technically difficult due to potential atomic coalescence [142–144]. Alternatively, modifications of the porous frameworks based on the embedment of metal nanoparticles have been recently investigated, producing very impressive gas-capacity records [145–147].

III. DENSITY FUNCTIONAL THEORY METHODS

A. General considerations

The wave function of a N -electron system, $\Psi(\mathbf{r}_1, \mathbf{r}_2, \dots, \mathbf{r}_N)$, contains all its physical information and it is determined by solving the corresponding Schrödinger equation. In real materials electrons interact through the Coulomb repulsion and are abundant, thus Ψ is a complex mathematical function that in most of the cases is unknown. In 1965, Kohn-Sham developed an ingenious theory to effectively calculate the energy and related properties of many-electron systems without the need of explicitly knowing Ψ [148, 149]. The main idea underlying this theory, called density functional theory (DFT), is that the exact ground-state energy, E , and electron density, $n(\mathbf{r})$, of a many-electron system can be determined by solving an effective one-electron Schrödinger equation of the form:

$$H_{eff}\psi_{i\sigma} = \epsilon_{i\sigma}\psi_{i\sigma} , \quad (1)$$

where index i labels different one-electron orbitals and σ the corresponding spin state. In particular,

$$H_{eff} = -\frac{1}{2}\nabla^2 + V_{ext}(\mathbf{r}) + \int \frac{n(\mathbf{r}')}{|\mathbf{r} - \mathbf{r}'|} d\mathbf{r}' + V_{xc}(\mathbf{r}) , \quad (2)$$

and

$$n(\mathbf{r}) = \sum_{i\sigma} |\psi_{i\sigma}(\mathbf{r})|^2 , \quad (3)$$

where V_{ext} represents an external field and $V_{xc}(\mathbf{r}) = \delta E_{xc} / \delta n(\mathbf{r})$ is the potential function that results from deriving the exchange-correlation energy, E_{xc} , with respect to the electron density.

The exchange-correlation energy has a purely quantum mechanical origin and can be defined as the interaction energy difference between a many-electron quantum system and its classical counterpart. Electrons are indistinguishable particles called fermions and the wave function

describing an ensemble of electrons must change its sign when two particles exchange orbital states. This quantum antisymmetry leads to an effective repulsion between electrons, called the Pauli repulsion, which helps in lowering their total Coulomb energy. Despite E_{xc} represents a relatively small fraction of the total energy, this is an extremely crucial quantity for all the physical aspects of materials and molecules because it acts directly on the bonding of atoms. The $E_{xc}[n]$ functional generally is unknown and in practice needs to be approximated. Actually, this is the only source of fundamental error in DFT methods and depending on the approximation that is used the resulting approach may turn out to be valid or not for describing the systems and phenomena of interest.

In standard cases $E_{xc}[n]$ is approximated with the expression

$$E_{xc}^{approx}[n] = \int \epsilon_{xc}^{approx}(\mathbf{r}) n(\mathbf{r}) d\mathbf{r} , \quad (4)$$

where ϵ_{xc}^{approx} is made to depend on $n(\mathbf{r})$, $\nabla n(\mathbf{r})$, and/or the electronic kinetic energy $\tau(\mathbf{r}) = \frac{1}{2} \sum_{i\sigma} |\nabla \psi_{i\sigma}(\mathbf{r})|^2$ (see next sections). Actually, the exact form of the exchange-correlation energy is readily known and reads

$$E_{xc}[n] = \int n(\mathbf{r}) d\mathbf{r} \int \frac{n_{xc}(\mathbf{r}, \mathbf{r}')}{|\mathbf{r} - \mathbf{r}'|} d\mathbf{r}' , \quad (5)$$

where $n_{xc}(\mathbf{r}, \mathbf{r}') = n_x(\mathbf{r}, \mathbf{r}') + n_c(\mathbf{r}, \mathbf{r}')$ is the exchange-correlation hole density at position \mathbf{r}' that surrounds an electron at position \mathbf{r} . Some important constraints on $n_{xc}(\mathbf{r}, \mathbf{r}')$ have already been established. For instance, $n_x(\mathbf{r}, \mathbf{r}')$ must be nonpositive everywhere and its space integral is equal to -1 . Also, the space integral of the correlation hole density is zero. These constraints can be employed in the construction of approximate, but physically correct, $E_{xc}[n]$ functionals.

In the next subsections, we review the most popular $E_{xc}[n]$ approximations which are currently employed in computational studies of GAM. In Table I, we summarize the main types of bonded and nonbonded atomic interactions taking place in condensed matter systems and surfaces. In Table II, we outline the adequacy of the considered DFT methods in describing those interactions. In Table III, we list some popular computer simulation packages that can be used to perform standard and more advanced DFT calculations. Finally, the relative degree of accuracy and computational expense associated to those DFT approaches are sketched in Fig. 5. Additional details on these topics can be found in some recent specialized reviews [150–154].

B. Local and semi-Local E_{xc} energy functionals

In local approaches (e.g., local density approximation -LDA-), E_{xc} is approximated with Eq. (4) and the exchange-correlation energy is taken to be that of

Interaction type → Aspect ↓	Covalent	Ionic	Hydrogen bond	Dispersion	Many – body
Spatial decay	$\exp[-r^2]$	$\frac{1}{r}$	$\frac{1}{r^3}$	$\frac{1}{r^N}$ ($N \geq 6$)	System dependent
Energy scale (eV/molecule)	1.0 – 0.1	1.0 – 0.1	0.1	0.1 – 0.01	0.1 – 0.001

TABLE I. Characteristic traits of usual bonded and nonbonded atomic interactions taking place in condensed matter systems and surfaces.

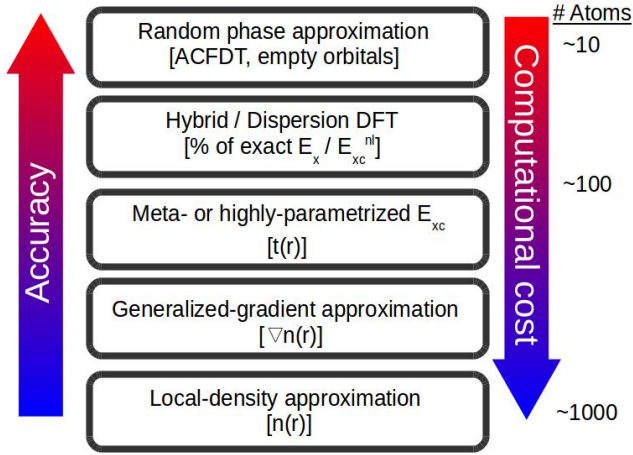


FIG. 5. Representation of common levels of E_{xc} approximation within density functional theory together with some general features. Regions coloured in red indicate “High” and in blue “Low”. The typical size of the systems that can be handled with those approaches are indicated on the right margin of the figure.

an uniform electron gas with density $n(\mathbf{r})$, namely ϵ_{xc}^{unif} . The exact expression of the $\epsilon_{xc}^{unif}[n]$ functional is known numerically from accurate quantum Monte Carlo calculations [35, 155]. In order to deal with the nonuniformity of realistic many-electron systems, these are normally partitioned into infinitesimal volume elements which are considered to be locally uniform. In semilocal approaches (e.g., generalized gradient approximation -GGA-), E_{xc} is approximated also with Eq. (4) and ϵ_{xc}^{approx} is made to depend on $n(\mathbf{r})$ and its gradient $\nabla n(\mathbf{r})$ [156, 157].

Both local and semilocal approximations satisfy certain exact E_{xc} constraints (e.g., some exact scaling relations and the exchange-correlation hole sum rules) and can work notably well for systems in which the electronic density varies slowly over space (e.g., bulk crystals at equilibrium conditions, see Table II). However, this is manifestly not the case of GAM which normally contain surfaces and pores where $n(\mathbf{r})$ can change very abruptly. Moreover, by construction local and semilocal functionals totally neglect long-range electron correlations, oth-

erwise known as dispersion interactions, which certainly are ubiquitous in gas-adsorption phenomena.

C. Meta-GGA or highly parametrized E_{xc} energy functionals

Meta-GGA functionals are semilocal in nature (i.e., assume the approximate $E_{xc}[n]$ expression in Eq. (4) but contain an additional degree of elaboration with respect to LDA and GGA: the orbital kinetic energy density, $\tau(\mathbf{r}) = \frac{1}{2} \sum_{i\sigma} |\nabla \psi_{i\sigma}(\mathbf{r})|^2$. This new ingredient allows one to construct functionals which satisfy some additional exact constraints, like for instance the correct gradient expansion of the exchange energy up to fourth order. Another interesting feature of this family of functionals is that they can be trained to capture the short- and middle-range parts of electronic correlation, which in some special cases may be enough to describe correctly the binding of atoms (see Table II).

Meta-GGA functionals are versatile and in general do not entail significantly larger computational expense than standard LDA and GGA. Examples of this family include the suite of TPSS functionals due to Perdew, Scuseria, and others [158, 159], and the “Minnesota functionals” (MX, with $X = 05, 06, 08, 11$, and 12) developed by Truhlar and his group in the University of Minnesota [160]. Meta-GGA functionals in general can provide accurate lattice constants in solids, surface energies, and molecular binding energies, and are already implemented in popular quantum chemistry and DFT packages like, for instance, GAUSSIAN [161], NWCHEM [162], SIESTA [163], and VASP [164] (see Table III). Nevertheless, dispersion interactions cannot be reproduced systematically with these functionals since they lack of explicit nonlocal correlation kernels (see Sec. III E below).

D. Hybrid exchange energy functionals

Hybrid functionals comprise a combination of nonlocal exact Hartree-Fock (HF) and local exchange energies, together with semilocal correlation energies. The proportion in which both nonlocal and local exchange densi-

ties are mixed generally relies on empirical rules. The popular B3LYP [165], for instance, takes a 20 % of the exact HF exchange energy and the rest from the approximate GGA and LDA functionals. Other well-known hybrid functionals are the HSE proposed by Heyd-Scuseria-Ernzerhof [166], PBE0 [167], and the family of Minnesota meta hybrid GGA [160].

In contrast to local and semilocal functionals, hybrids describe to some extent the delocalization of the exchange-correlation hole around an electron. This situation becomes of particular relevance in chemisorption and charge transfer processes, where the atomic bonds turn out to be elongated or shortened. Also, in strongly correlated systems containing d and f electronic orbitals life, for instance, transition metal oxides. In other words, hybrid functionals are useful in situations where the electron self-interaction errors, stemming from an imperfect cancellation between the artificial interaction of an electron with itself and the exchange energy, are potentially large. Hybrid functionals, however, do not account for the long range part of the correlation hole energy and thus cannot reproduce dispersion forces (see Table II). Efforts to effectively correct for such drawbacks have been made recently by Head-Gordon and other authors (e.g., the range separated and dispersion corrected ω B97X-D and ω M06-D3 functionals) [168–171].

E. Dispersion-corrected E_{xc} energy functionals

The condition that any DFT-based dispersion scheme must accomplish is to reasonably reproduce the asymptotic $1/r^6$ behaviour of the interaction between two particles separated by a distance r in a gas. Local, semilocal, and hybrid energy functionals totally miss this requirement. The most straightforward way to correct for such a fault consists in adding an energy term to the exchange-correlation energy that is attractive and has the form $E_{\text{disp}} = -\sum_{i,j} C_{ij}/r_{ij}^6$ (where indexes i and j label different particles, and a damping factor is introduced at short distances in order to avoid divergences). This approximation represents the core of a suite of methods termed DFT-D which, due to their simplicity and low computational cost, are being widely used at the moment. Probably, the most popular family of DFT-D methods are the dispersion corrected GGA functionals proposed by Grimme [172]. Despite their appealing features, DFT-D methods present several shortcomings. First, many-body dispersion effects and faster decaying terms such as the B_{ij}/r_{ij}^8 and C_{ij}/r_{ij}^{10} interactions are completely disregarded. Second, it is not totally clear from where one should obtain the optimal C_{ij} coefficients. And finally, once these parameters are determined they remain fixed during the simulations, and this can be problematic in situations where the orbital hybridization and oxidation states change as compared to the free atoms case.

Several improvements on DFT-D methods have been proposed, in which the value of the dispersion coefficients

are made to depend on the specific atomic environment. Those correspond to the DFT-D3 method by Grimme [173], the vdW(TS) approach by Tkatchenko and Scheffler [174], and the BJ model by Becke and Johnson [175]. In those approaches the specific variation of the C_{ij} parameters are taken on the atomic coordination or effective volume, and the calculation of reference dispersion coefficients and atomic polarizabilities are required.

A third degree of elaboration exists in which no external input parameters are needed and the dispersion interaction is directly computed from the electron density. In this context, the exchange-correlation energy is expressed as $E_{xc} = E_x^{\text{GGA}} + E_c^{\text{LDA}} + E_c^{\text{nl}}$ where E_c^{nl} is the nonlocal correlation energy. Particularly, E_c^{nl} is calculated with a double space integral involving the electron density and a two-position integration kernel, ϕ , of the form

$$E_c^{\text{nl}}[n] = \frac{1}{2} \iint n(\mathbf{r}') \phi(q', q, |\mathbf{r}' - \mathbf{r}|) n(\mathbf{r}) d\mathbf{r}' d\mathbf{r} . \quad (6)$$

In Eq. (6), q' and q are the values of an universal function evaluated in positions \mathbf{r}' and \mathbf{r} , and ϕ is a complex function that obeys two main constraints: E_c^{nl} is strictly zero for any system with constant n , and the interaction between two molecules has the correct $|\mathbf{r}' - \mathbf{r}|^{-6}$ dependence for long distances. The described approach was introduced by Dion *et al.* in 2004 [176] and it represents a key DFT development since it combines all types of interaction ranges within a same formula. Refinements on Dion's approach have subsequently appeared where (i) the original two-position integration kernel ϕ is modified (e.g., the so-called nonlocal VV10 functional due to Vydrov and Voorhis [177–179]), and (ii) the exchange term in E_{xc} is substituted with other more accurate functionals (e.g., the so-called vdW-DF2 [180], vdW-optB88 and vdW-optPBE [181], and vdW-C09_x [182] schemes). All these approaches are termed vdW-DF and, thanks to the seminal work of Román-Pérez and Soler [183], their accompanying computational expense in a planewave framework is moderate in practice. Nevertheless, the way in which nonlocal correlations are calculated inherently assumes pairwise additivity and thus many-body effects are completely disregarded in vdW-DF methods (see Table II).

F. The random phase approximation and DFT+MBD

The adiabatic connection fluctuation-dissipation (ACFD) theorem provides a general and exact expression for the exchange-correlation energy of a many-electron system, thereby E_{xc} in principle can be calculated in a very accurate way incorporating higher-order many-body effects. In particular, the

Interaction type → DFT flavour ↓	Covalent	Ionic	Hydrogen bond	Dispersion	Many – body
Local and semi – local (LDA, GGA) [35, 155–157]	✓	✓	✓/×	×	×
Highly parametrized (Meta – GGA, Minnesota) [158–160]	✓	✓	✓/×	✓/×	×
Hybrid (B3LYP, HSE) [165–167]	✓	✓	✓	×	×
Dispersion – corrected (DFT – D2, vdW – DF, VV10) [172, 176, 177, 180, 181]	✓	✓	✓	✓	×
Many – body (DFT + MBD, RPA – DFT) [48, 49, 152, 153]	✓	✓	✓	✓	✓

TABLE II. Description of the performance of some DFT variants in describing usual types of bonded and nonbonded interactions found in condensed matter systems and surfaces. Symbol ✓ (×) indicates correct (incomplete) description of the considered type of interaction by the corresponding DFT method.

correlation energy of a system adopts the form

$$E_c = -\frac{1}{2\pi} \int_0^\infty d\omega \times \int_0^1 \mathbf{Tr} \left[\frac{\chi_\lambda(\mathbf{r}', \mathbf{r}, i\omega) - \chi_0(\mathbf{r}', \mathbf{r}, i\omega)}{|\mathbf{r}' - \mathbf{r}|} \right] d\lambda, \quad (7)$$

where $\chi_0(\mathbf{r}', \mathbf{r}, i\omega)$ is the bare density-density response function, $\chi_\lambda(\mathbf{r}', \mathbf{r}, i\omega)$ the interacting density-density response function at Coulomb coupling strength λ , and \mathbf{Tr} denotes the six-dimensional integration over the variables \mathbf{r}' and \mathbf{r} . The response function χ measures the electronic response of the system at a point \mathbf{r}' due to a frequency-dependent electric field perturbation at a point \mathbf{r} . In the ACFD approach, the adiabatic connection between a reference non-interacting system (defined at $\lambda = 0$) and the fully interacting system (defined at $\lambda = 1$) provides the correlation energy of the latter, including many-body dispersion as well as other types of electron correlation effects. This theoretical framework has been exploited by several authors to develop novel many-body DFT-based approaches, among which we highlight the random phase approximation to DFT and the DFT+MBD method.

In the random phase approximation (RPA-DFT) scheme, the interacting response function χ_λ is defined self-consistently via the equation $\chi_\lambda = \chi_0 + \lambda \frac{\chi_0 \chi_\lambda}{|\mathbf{r}' - \mathbf{r}|}$. This approximation has been shown to work reasonably well for a number of cluster and extended systems [184]. Following the Adler-Wiser formalism [185, 186], χ_0 can be

computed by using the occupied and virtual orbitals, and the corresponding energies and occupancies obtained in DFT calculations. In analogy to post-HF approaches, the computational expense associated to RPA-DFT is very large (i.e., typically scales with the fourth power of the number of particles) and the convergence with respect to the basis set generally is too slow [187–191]. Also, it must be noted that the short-range part of the electron correlation energy is not precisely reproduced by RPA-DFT and that this shortcoming may be problematic in studying molecular systems [192].

Meanwhile, recent efforts done in the groups of Tkatchenko and Scheffler have given birth to the so-called DFT+MBD method [47–50], which accounts also correctly for the Coulomb screening and many-body effects in electronic systems. In the DFT+MBD approach, the Schrödinger equation of a set of fluctuating and interacting quantum harmonic oscillators is solved directly within the dipole approximation, and the resulting many-body energy is coupled to an approximate semilocal DFT functional. These approximations result in a significant reduction of computational load as compared to the RPA-DFT method, allowing one to describe larger systems containing up to few hundreds of atoms.

The most appealing features of the RPA-DFT and DFT+MBD methods is that they are very accurate and suitable for studying small-gap and metallic periodic systems. In fact, these techniques have already been ap-

plied successfully to the study of strongly correlated crystals and surfaces [193–195], organic molecules adsorbed on metallic surfaces [47], and ionic and semiconductor solids [196]. Effective schemes of the RPA-DFT and DFT+MBD methods have already been implemented in commercial and open-source first-principles packages like, for instance, ABINIT [197], GPAW [203], and VASP [164] (see Table III).

IV. ASSESSING THE PERFORMANCE OF DFT METHODS IN THE DESIGN OF GAM

Making judicious comparisons between zero-temperature calculations and ambient-temperature observations turns out to be very complicated due to the presence of thermal excitations. Temperature profoundly affects the (free) energy and conformation of molecules adsorbed on GAM, and the differences with respect to $T = 0$ conditions are difficult to assess with theory even when considering the simplest interaction models. In fact, free energies and entropies cannot be accessed straightforwardly during molecular dynamic simulations, in contrast to other thermodynamic quantities like, for instance, the total internal energy and pressure. In order to evaluate free energies technically and computationally involved methods like thermodynamic integration, free-energy perturbation and umbrella sampling, have to be employed [207–210]. Reasonably then, the most direct and exact way of evaluating the performance of approximate ground-state methods is to compare them with other computational approaches which are known to be more accurate. In the case of DFT methods, accuracy benchmark tests involve the application of quantum chemistry methods (QCM) like Møller-Plesset perturbation theory (MP2), the coupled-cluster method with single, double and perturbative triple excitations [CCSD(T)], and quantum Monte Carlo (e.g., diffusion Monte Carlo -DMC-).

In what follows, we review recent DFT benchmark studies done in the areas of hydrogen storage and carbon capture and sequestration problems involving CN and MOF. Based on them, we draw general conclusions on the suitability of approximate exchange-correlation functionals for the design of GAM. Regrettably, despite that the number of these benchmark studies is very modest, as it will be shown next, some interpretation and computational inconsistencies prevail yet among them. Also, we discuss the subtle problems found in the generalization of DFT performance tests done in model cluster systems to extended GAM. A few modeling strategies are proposed to overcome this class of problems, some of which are computationally very intensive and some others tentative.

A. H₂ storage

1. Carbon-based GAM

A promising alternative to functionalizing carbon-based GAM with transition metals atoms is to use alkali metal species like lithium and calcium. Aggregation issues on alkali metal coatings are expected to be less severe than in the transition metal case (see Sec. II B), and the corresponding H₂ gravimetric densities predicted in DFT studies largely surpass the targets set by the U.S. Department of Energy (i.e., 5.5 wt. %) [134, 211, 212]. Reported experimental records, however, lie significantly below the impressive performances anticipated with theory (e.g., a modest 2 wt. %) [213–216] and the reasons for those large discrepancies are not yet totally understood.

In 2009, Cha *et al.* published a controversial work in which the accuracy of standard DFT methods in the assessment of H₂-storage GAM was seriously questioned [217]. By using quantum chemistry [i.e., MP2 and CCSD(T)] and standard and hybrid DFT methods, Cha showed that the binding energies, E_{bind} , and interatomic distances calculated in a model system composed of four equidistant hydrogen molecules to a positively charged Ca ion [i.e., $\text{Ca}^+(\text{H}_2)_4$, see Fig. 6a], were dramatically different. In particular, with standard and hybrid DFT functionals favorable molecular binding to the calcium cation (i.e., E_{bind} values around ~ -1.0 and -0.1 eV) was found at a H₂-Ca⁺ distance of $z = 2.3$ Å, whereas with MP2 and CCSD(T) methods no effective binding was determined at any separation (see Table IV). Cha *et al.* performed analogous gas-adsorption calculations in a larger system comprising a coronene molecule (i.e., C₂₄H₁₂) and a calcium atom, and concluded with the same level of inconsistency that found in the $\text{Ca}^+(\text{H}_2)_4$ case. In words of Cha *et al.* [217]: “(these findings) indicate that previous suggestions for the Ca-based hydrogen storage system should be reinvestigated with particular care about the charge state of Ca”. The levels of alarm associated with this error class, however, were lowered shortly afterwards by Ohk *et al.*. In a formal comment on Cha’s work, Ohk argued that the discrepancies between MP2 and DFT methods reported in the $\text{Ca}^+(\text{H}_2)_4$ and Ca-C₂₄H₁₂ systems were numerical artifacts stemming from the use of small localized orbitals basis sets, i.e., $6 - 311 + G^{**}$, which did not contain polarization functions of high enough momenta [218]. By using larger basis sets of the Dunning type and performing extrapolation to the complete basis set (CBS) limit to get rid of likely finite basis-set errors, Ohk *et al.* showed that the agreement between semilocal DFT and MP2 results obtained in Ca-decorated cluster models was qualitatively acceptable (although standard DFT methods exhibited a strong tendency towards molecular overbinding, see Table IV). The reliability of GGA functionals in the assessment of hydrogen storage materials apparently had it been restored (at least, at the qualitative level). However, a deep understanding about how standard DFT function-

Package	Periodic/Basis set	Standard	Meta – GGA	Hybrid	Dispersion – corrected	Many – body
ABINIT [197]	✓/PW	✓	✓	✓	✓	✓
ADF [198]	✓/STO	✓	✓	✓	✓ (× vdW – DF)	×
CASTEP [199]	✓/PW	✓	✓	✓	✓ (× vdW – DF)	×
CP2K [200]	✓/GTO, PW	✓	✓	✓	✓	×
CRYSTAL [201]	✓/GTO	✓	✓	✓	✓ (× vdW – DF)	×
GAMESS [202]	×/GTO	✓	✓	✓	✓ (× vdW – DF)	×
GAUSSIAN [161]	✓/GTO	✓	✓	✓	✓ (× vdW – DF)	×
GPAW [203]	✓/NAO, PW	✓	✓	✓	✓	✓
MOLPRO [204]	×/GTO	✓	✓	✓	×	×
NWCHEM [162]	✓/GTO, PW	✓	✓	✓	✓ (× vdW – DF)	×
EXPRESSO [205]	✓/PW	✓	✓	✓	✓	×
SIESTA [163]	✓/NAO	✓	✓	✓	✓	×
VASP [164]	✓/PW	✓	✓	✓	✓	✓
WIEN2K [206]	✓/FP – (L)APW + lo	✓	✓	✓	✓ (× vdW – DF)	×

TABLE III. Selected computer packages which can be used to perform DFT calculations. “Periodic” refers to the ability of handling the simulation of three-dimensional periodic systems. In “Basis set”, “PW” refers to plane waves, “STO” to Slater-type orbitals, “GTO” to Gaussian orbitals, “NAO” to numerical atomic orbitals, and “FP-(L)APW+lo” to augmented plane waves and local orbitals. Symbol ✓ (×) indicates suitability (unsuitableness) of the package to perform a particular calculation type.

als, which definitely incur in self-interaction errors and neglect long-range dispersive interactions, could describe the adsorption of light molecules on surfaces and cavities correctly, was still missing.

In two subsequent works, the authors of article [217] reported further details on the anomalous performance of customary DFT methods in describing the fixation of H_2 molecules on Ca centers via the Kubas interaction [219, 220]. They showed that when a sharp orbital transition occurs during adsorption of the gas molecule on the metal center, the incompleteness of the electronic exchange, present in most DFT functionals, acts critically by providing erroneous over stabilization of the final complex. According to Cha *et al.*, $Ca^+(H_2)_4$ exemplifies the type of system where the highest occupied molecular orbital (HOMO) changes abruptly from $4s$ to $3d$ character upon the intake of gas, and the fixation of H_2 molecules via the Kubas interaction becomes frustrated. Cha’s explanations are based on arguments put forward by Gunnarsson more than two decades ago, who

showed that in situations where the nodal wavefunction surfaces are intricate approximate DFT exchange functionals tend to be imprecise by underestimating the energy cost associated to orbital transitions [221]. Cha’s arguments indeed brought new physical insight into the $Ca^+(H_2)_4$ contention, however some technical aspects of works [219, 220] could still be criticized (e.g., extrapolation to the CBS limit in the MP2 calculations was not pursued). Thus, further benchmark studies were still required for carefully judging the accuracy of customary DFT methods in the design of carbon-based GAM.

In this regard, Bajdich *et al.* made an important contribution by performing for the first time quantum Monte Carlo (QMC) calculations in the $Ca^+(H_2)_4$ model system, and comparing their results to those obtained with the MP2, and local, semilocal and hybrid DFT methods [222] (see Table IV). It was found that QMC calculations based on the diffusion Monte Carlo (DMC) predicted no binding at all of the four H_2 molecules to the Ca^+ center within the interval $0 \leq z \leq 4.6 \text{ \AA}$, in agree-

Work	E_{bind} (eV/H ₂)	z_{min} (Å)	$d_{\text{H-H}}$ (Å)	Method
[217]	-1.50	2.3	0.81	LDA/6 - 311 + +G **
	-0.30	2.3	0.78	PBE/6 - 311 + +G **
	-0.40	2.3	0.77	B3LYP/6 - 311 + +G **
	-0.05	4.2	0.74	MP2/6 - 311 + +G **
	-0.05	4.2	0.74	CCSD(T)/6 - 311 + +G **
[218]	-0.90	2.3		PBE/cc - pVQZ
	-0.20	3.4		MP2/cc - pVQZ
	-0.15	2.3		CCSD(T)/CBS
[222]	-1.20	2.3	0.77	LDA
	-0.70	2.3	0.77	PBE
	-0.30	2.3	0.77	B3LYP
	No binding	$z \leq 4.6$	0.77	MP2
	No binding	$z \leq 4.6$	0.77	HFx - PBEc
	No binding	$z \leq 4.6$	0.77	DMC/ANO - VTZ
[223]	-0.16	3.5	0.74	MP2/CBS
	-0.18	2.2/3.4	0.77	AF - QMC/CBS

TABLE IV. Summary of the binding energy and structural results obtained in the $\text{Ca}^+(\text{H}_2)_4$ model cluster system by different authors employing a variety of DFT and quantum chemistry methods (see text).

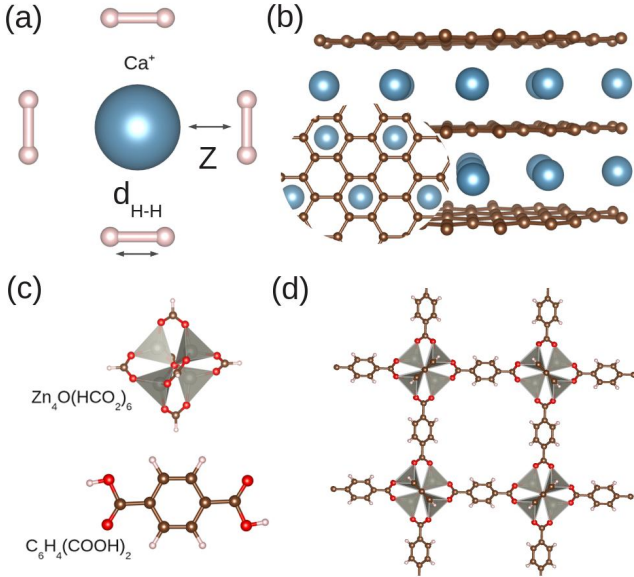


FIG. 6. Sketch of the (a) $\text{Ca}^+(\text{H}_2)_4$ model cluster system, (b) graphite intercalation compounds [123–125] seen from the front and top views, (c) organic connector and metal cluster model systems, and (d) MOF-5 [also known as IRMOF-1]. Cluster systems in (a) and (c) have been widely considered in benchmark studies as representative models of GAM depicted in (b) and (d), respectively.

ment with previous MP2 results. In stark contrast to this conclusion, popular DFT functionals like LDA, GGA and B3LYP vaticinated effective fixation of the gas molecules at a distance of 2.3 Å. Bajdich’s results are in qualitative agreement (disagreement) with Cha’s (Ohk’s) conclusions explained above. Interestingly, the authors of work [222] carried out DFT calculations with a blended functional consisting of the full HF exchange energy and the PBE correlation functional (denoted as HFx-PBEc in Table IV). They showed that the results obtained with the HFx-PBEc functional were consistent with those obtained with the MP2 and DMC methods (see Table IV). In light of those outcomes, Bajdich *et al.* argued that the failure of common DFT functionals in describing the $\text{Ca}^+(\text{H}_2)_4$ system had its origins on the partial or total omission of long-range exchange interactions, in coincidence with Cha’s reasonings found in works [219, 220]. In spite of the significance of Bajdich’s work, this is neither free of some technical objections. For instance, in the atomic relaxations the H-H intermolecular distances were kept fixed to 0.77 Å, and the errors stemming from the incompleteness of the employed basis sets (i.e., triple-zeta) and the fixed-node surface approximation in DMC, were not evaluated.

In a posterior work, Purwanto *et al.* presented a highly accurate study on the binding of the $\text{Ca}^+(\text{H}_2)_4$ complex which relied on auxiliary-field QMC calculations [223].

There, extrapolation to the complete basis set limit and a better treatment of the sign problem were accomplished. Purwanto *et al.* found that the potential energy curve of the four hydrogen molecules exhibits a double-well structure with almost equal binding minima of ~ -0.18 eV at distances 2.2 and 3.4 Å. These results are in good agreement with the MP2/CBS calculations performed by the same authors and the CCSD(T)/CBS results obtained by Ohk *et al.* [218] (see Table IV). Regarding the differences with respect to Bajdich’s work, it was argued that these were likely to be originated by the fixed-node approximation employed in the DMC calculations.

Conclusions.- The main conclusion emerging from works [217–220, 222, 223] is that standard DFT functionals tend to overestimate the cohesion of the $\text{Ca}^+(\text{H}_2)_4$ complex, and that the likely reason for this flaw is a deficient treatment of the long-range exchange energy. On the other hand, highly accurate QCM results obtained by different groups on the same system are not fully consistent and therefore a conclusive verdict on the general performance of DFT methods, i.e., considering all its possible flavours, cannot be emitted. The current status of computational work on this topic is clearly unsatisfactory.

Yet, the situation becomes even more puzzling when the resemblance between the model system $\text{Ca}^+(\text{H}_2)_4$ and real carbon-based H_2 -storage GAM is brought into examination (e.g., see Fig. 6a-b). Namely, there is still the unresolved question about on which grounds the results obtained in model cluster systems can be translated (if possible at all) to realistic extended materials [55, 56]. For instance, the likely presence of valence *s* and *p* electronic states, coming from the carbon atoms in the sorbent, is totally disregarded in the $\text{Ca}^+(\text{H}_2)_4$ complex. Also, the role of the long-range dispersion interactions, which are ubiquitous in gas-adsorption processes, normally turns out to be underestimated in nano-sized systems. In this last regard, several analysis on the hydrogen storage properties of extended Ca-decorated carbon nanomaterials based on dispersion-corrected DFT functionals, have been reported recently.

Wang *et al.* have studied the H_2 -storage properties of Ca-decorated graphene with the vdW-DF approach due to Dion [176] and compared their results to those obtained with standard local and semilocal methods [224]. Wang’s calculations show that the H_2 binding energies obtained with the vdW-DF method lie systematically below those obtained with GGA-PBE (i.e., stronger molecule-GAM interactions by ~ 0.05 eV/molecule), and generally above the LDA results (i.e., weaker molecule-GAM interactions by $\sim 0.05 - 0.10$ eV/molecule). (Similar conclusions have been attained by other authors in alike Ca-decorated carbon nanomaterials [225, 226].) In light of these outcomes, it is argued that long-range dispersion interactions can be also important in the adsorption of hydrogen molecules on chemically modified carbon nanomaterials, even in the cases where the obtained binding energies are large (i.e., $|E_{\text{bind}}| \geq 0.1$ eV/molecule).

Actually, Wang’s results appear to expose a new failure of standard DFT methods in the assessment of GAM, this time related to the description of the electronic correlation energy. Unfortunately, the authors of work [224] did not report any comparison with respect to hybrid functionals or QCM calculations, hence the size of the bias incurred by the vdW-DF method itself, i.e., due to the approximations performed on the exchange functional and pairwise additivity, cannot be inferred.

In work [227], Wong *et al.* have investigated also the adsorption of H_2 molecules on metal-decorated graphene but considering a large set of transition and alkali metal species. The employed method there is an improved version of Dion’s approach, the so-called vdW-DF2, in which the accuracy of the employed semilocal exchange functional is bettered [180]. In the case of Ca-based coatings, Wong’s results are in qualitative agreement with those obtained by Wang *et al.* [224] however the difference between the two reported vdW-DF and vdW-DF2 H_2 -binding energies is not negligible (i.e., about 30 meV). When considering other types of dopants, vdW-DF2 calculations generally predict weaker molecular binding than obtained with semilocal GGA methods by ~ 0.1 eV per molecule. In fact, Wong’s work comes to reinforce the idea that dispersion interactions can affect profoundly the interplay between extended materials and hydrogen molecules. Consequently, nonlocal correlations must be taken into account by any DFT functional that is intended for modeling of GAM.

Conclusions.- From all these benchmark studies, we can draw the general conclusion that both long-range exchange and dispersion electronic interactions are pivotal in describing the binding of H_2 molecules to CN-based GAM. As for local and semilocal DFT functionals, these two elements are totally missing in them, therefore they are likely to provide unreliable results on the hydrogen storage topic. Situations in which local and semilocal GAM predictions seem to be correct normally are fortuitous and indicate the presence of large energy error cancellations [225, 226]. Namely, the sign of the missing contributions to the exchange-correlation energy in local and semilocal approaches are opposite and therefore can compensate each to the other. These error cancellations, however, do not occur systematically and may depend on the specific details of GAM (e.g., see work [227] where the sign of the difference between the GGA and vdW-DF2 energies varies with the dopant species), and thus the use of standard DFT methods for modeling of carbon-based H_2 -storage materials is not recommended. Meanwhile, new quantum Monte Carlo (QMC) and RPA-DFT simulations, this time performed in periodic systems, are highly desirable for rigorously evaluating the performance of meta, hybrid, and dispersion DFT functionals (see works [152, 195, 228–230] for examples of applications of such advanced computational methods to simulation of relevant materials). QMC and RPA-DFT calculations are also necessary for determining the relevance of many-body energy and Coulomb screening ef-

fects on the present class of GAM, which so far have been systematically neglected.

2. MOF

The interplay between H_2 molecules and MOF (e.g., MOF-74,5) are dominated by dispersion interactions and the local environment surrounding the binding sites in the metal clusters [231–234]. Consequently, employing DFT methods that completely neglect nonlocal correlations (i.e., standard and hybrid flavours) and/or carrying out benchmark tests in model cluster systems which are too small (see Fig. 6c-d) turns out to be inadequate in the present case. On the other side, the fact that the H_2 -MOF interactions are weak implies that effective gas-storage can only be achieved at temperatures well below ambient conditions (i.e., $T \sim 80$ K). Thus, a number of strategies have been proposed for increasing the affinity of MOF towards hydrogen binding [235]. These include, the design and control of porosity [236], functionalization of the organic linkers [237], hydrogen spillover [114, 115], introduction of open metal sites in the organic linkers and metal clusters [142, 238–241], and decoration of MOF surfaces with alkali metal atoms [242–244]. DFT methods have been intensively employed in the last two mentioned approaches hence we revise next the benchmark tests undertaken in those areas.

It was first argued by Lochan *et al.* that H_2 molecules are attracted by open transition metal and alkali centers in MOF through donor-acceptor interactions and electrostatics [238]. Based on the outcomes of standard DFT calculations, those authors concluded that the strength of the H_2 -MOF interactions was within the range of desirable binding for ambient gas storage applications (i.e., 0.3 – 0.8 eV). Lochan *et al.* also claimed that semilocal DFT functionals could be *safely* employed in the study of H_2 -MOF systems because the corresponding leading electronic interactions are strong and predominant over dispersion [238].

In two recent studies, Sun *et al.* have evaluated the accuracy of standard, hybrid and meta DFT functionals in the prediction of H_2 adsorption on metal-doped organic linker systems [245, 246]. They have found that whenever transition metal, alkaline-earth or alkali metal atoms are used, all DFT, MP2 and CCSD(T) methods provide quantitatively similar binding energy results, in satisfactory accordance with Lochan’s findings (see Table V). In particular, calculations performed with popular DFT functionals like PBE, PW91 and M05-2X are in excellent agreement with gold-standard benchmarks obtained with the CCSD(T) method (i.e., equal binding energies to within ~ 0.01 eV). Meanwhile, hybrid functionals tend to underestimate E_{bind} slightly by 0.05 – 0.10 eV. Analogous conclusions have been attained also by Dixit *et al.* in a posterior work done in Li-decorated MOF (see Table V) [247].

A further benchmark test confirming the accuracy of

DFT methods in describing the interplay between H_2 molecules and chemically functionalized organic linkers, has been recently reported by Jiang *et al.* [248]. In particular, Jiang *et al.* have studied the binding of a hydrogen molecule to a small C_4H_3Li cluster using common GGA and hybrid DFT functionals, and the highly accurate DMC method. As it can be appreciated in Table V, notable agreement between all the considered approaches in Jiang’s calculations is obtained (i.e., within ~ 0.01 eV).

Conclusions.— In light of the benchmark results reported in works [245–248], we may conclude that customary DFT methods appear to perform appropriately in the simulation of the hydrogen-storage properties of chemically functionalized MOF. The physical reason underlying this favorable outcome is that donor-acceptor interactions and electrostatics in this family of GAM are dominated by short- and medium-range electron-electron exchange and correlations. Nevertheless, a note of caution must be added here.

In our compilation of benchmark tests we have realized a lack of studies analyzing the performance of dispersion-corrected DFT schemes in the simulation of extended hydrogen-loaded MOF containing open metal sites. Indeed, dispersion interactions appear to be secondary in the present case however, as we will show in Sec. IV B 2, when H_2 molecules are replaced by CO_2 this type of interactions turns out to be crucial. The polarizability of the H_2 molecule certainly is smaller than that of CO_2 (0.79 and 2.51 \AA^3 , respectively [249]), however this still must have some effect. Actually, it would be very interesting to quantify in which proportion dispersion interactions tend to lower the DFT energies reported in Table V (which, we remind, have been obtained in model cluster systems). Also, it would be highly desirable to perform systematic studies on the performance of local, semilocal, and nonlocal DFT approaches in periodic simulation of chemically functionalized MOF loaded with hydrogen. In this regard, we would like to mention a recent work by Sumida *et al.* in which it has been shown that neither standard nor hybrid DFT functionals can reproduce with accuracy the measurements done on the binding of H_2 molecules to metal-BTT [250]. Rather, a range-separated hybrid and dispersion corrected DFT functional, i.e., the so-called $\omega B97X-D$ (see Sec. III D), is found to be necessary for a correct interpretation of the experimental findings (see for instance Table II in work [250]). Also, Kong *et al.* have recently found that nonlocal interactions are crucial to achieve DFT consistency with respect to the H_2 heats of adsorption measured in $Zn_2(BDC)_2(C_6H_{12}N_2)$ [251]. Further DFT work on the role of the dispersion interactions in hydrogen storage of chemically functionalized MOF, is urgently needed in order to avoid likely modeling inconsistencies.

Work	System	E_{bind} (eV/H ₂)						
		PW91	PBE	B3LYP	M05 - 2X	MP2	CCSD(T)	DMC
[245]	H ₂ - Ca@H ₄ B ₂ C ₆ O ₄		-0.16			-0.16 (CBS)		
[246]	H ₂ - Ca@C ₈ H ₆ O ₄	-0.22	-0.19	-0.15	-0.26	-0.26 (CBS)	-0.24 (CBS)	
[246]	H ₂ - Sc@C ₅ H ₅	-0.28	-0.27	-0.14	-0.23	-0.24 (CBS)	-0.23 (CBS)	
[246]	H ₂ - Ti@C ₂ H ₄	-0.39	-0.37	-0.26	-0.38	-0.42 (CBS)	-0.37 (CBS)	
[246]	H ₂ - Li@C ₈ H ₆ O ₄	-0.15	-0.13	-0.10	-0.16	-0.16 (CBS)	-0.16 (CBS)	
[247]	H ₂ - Li@C ₁₀ H ₁₀ O ₄	-0.42 (cc - pVTZ)	-0.18	-0.16 (cc - pVTZ)		-0.17 (cc - pVTZ)		
[248]	H ₂ - Li@C ₄ H ₃	-0.11	-0.12	-0.12 (6 - 311G[d, p])				-0.14

TABLE V. Results of different benchmark tests carried out in organic linker MOF models decorated with alkaline earth, alkali and transition metal atomic species. The types of localized-orbitals basis sets employed in the calculations and the cases in which convergence to the CBS limit is achieved, are indicated within parentheses.

B. CO₂ capture and sequestration

1. Carbon-based GAM

The adsorption of CO₂ molecules on carbon-based GAM can be of physisorption or chemisorption type depending on whether the material surfaces are smooth, contain defects or are chemically functionalized. In the case of nondefective surfaces, the interactions with the gas molecules are dominated by dispersion forces thereby the gas is retained on the adsorbent material very weakly [252].

In 2006, Xu *et al.* were the first in carrying out nonstandard DFT calculations on the binding of CO₂ molecules to pristine graphene [253]. By using the hybrid ONIOM[B3LYP:DFTB-D] method, they found that the corresponding gas-adsorption energy was $E_{\text{bind}} = -0.03$ eV. In Xu's approach, an hybrid DFT evaluation of the interactions between CO₂ and a coronene molecule is first performed, and a tight-binding dispersion correction is subsequently added in order to account for the presence of π -conjugated interactions in the real material. More recently, Umadevi *et al.* have analyzed the same type of problem but employing meta-GGA DFT methods (i.e., M05-2X), and surprisingly they have found a large physisorption energy of ~ -0.10 eV [254]. The reasons for

the three-fold discrepancy between Xu's and Umadevi's results remain unclear to us since QCM benchmark calculations on the strength and nature of the CO₂-graphene or CO₂-coronene interactions are practically absent to date. We only know of a recent work [255] by Lee *et al.* in which the physisorption energy of CO₂ is calculated with the MP2 method. In this case, E_{bind} turns out to amount to -0.09 and -0.13 eV, depending on the relative orientation between the gas molecule and carbon plane. Nevertheless, the basis set of localized orbitals employed in Lee's study is relatively small (i.e., 6-31G**) and the model cluster system in which the MP2 calculations are performed contains carbon dangling bonds (in opposition to real graphene).

On the other side, the adsorption of gas molecules on carbon nanotubes (CNT) has been thoroughly analyzed by Quiñonero *et al.* with dispersion-corrected DFT methods (i.e., B97-D/SVP) [256]. By considering different types of CNT, diameters, and binding sites, Quiñonero *et al.* have concluded that CO₂-adsorption is energetically more favourable in the interior than in the exterior of nanotubes, in marked disagreement with previous reports [257, 258]. Also, they have found that the strongest CO₂-CNT interactions occur in the (9, 0) and (5, 5) systems where the computed binding energy amounts to ~ -0.6 eV. Interestingly, based on a symmetry-adapted perturbation theory (SAPT) decom-

position of the calculated DFT-D interaction energies, the authors of work [256] show that (i) dispersion interactions account for the 80 % of the total attractive forces, and (ii) electrostatic interactions resulting from the overlap between CO₂ and CNT electronic orbitals, although secondary, are yet important. We realize, however, a lack of high-level *ab initio* investigations, e.g., employing the MP2 and CCSD(T) methods, in the effects of the CNT size and curvature on the binding of CO₂ molecules. This type of studies would be highly desirable for a consistent evaluation of the performance of DFT methods on this topic. Similar investigations to these proposed have already been performed for methane [259], a molecule that is akin to carbon dioxide in terms of the electric dipole and quadrupole moments. It is worth noticing that during the preparation of this review we became aware of the submission of an article by Smith and Patkowski which could fill the mentioned knowledge gap in CO₂-CNT systems [260].

When the surfaces of the carbon nanomaterials contain reactive defect sites like vacancies, holes (i.e., clusters of vacancies) and edges, the interactions with CO₂ molecules become more intense. For instance, Cabrera-Sanfelix has studied the adsorption of carbon dioxide on a defected graphene sheet with standard DFT methods (i.e., DFT-GGA) and has found that molecular physisorption and chemisorption have an energy cost of -0.14 and -1.44 eV, respectively [261]. Similar results have been obtained by Liu *et al.* in an equivalent system using an analogous computational approach (i.e., -0.21 and -1.72 eV, respectively) [262]. However, the authors of this last study propose an equilibrium chemisorption configuration that is more symmetric than the one obtained by Cabrera-Sanfelix. In a more recent and technically exhaustive work, Wood *et al.* have addressed the same kind of gas-adsorption problem by employing both dispersion corrected DFT and MP2 methods [263]. Essentially, they find that DFT methods incorporating van der Waals forces provide adsorption energies which are in good agreement with MP2 results, and that CO₂ physisorption in the edges of a zigzag graphene nanoribbon occurs with an energy balance of -0.20 eV.

Conclusions.- In light of the results reported by Cabrera-Sanfelix, Liu, and Wood, we can conclude that using standard DFT methods for representing the interactions of CO₂ molecules with defected graphene seems to be appropriate. It is not clear to us, however, whether the suitability of DFT-GGA methods in this case corresponds to a large cancellation between errors or simply to a minor role played by the electronic long-range exchange and correlations.

Meanwhile, some functionalization techniques have been proposed for increasing the affinity of carbon-based GAM towards CO₂ binding, which is desirable for pre-combustion applications. Among those we highlight the decoration of carbon surfaces with nitrogen and light metal atoms, for which a number of experimental and first-principles computational works have been

performed [118, 264–270]. Mo *et al.* have recently presented a computational benchmark study of the adsorption of carbon dioxide on nitrogen-containing hydrocarbon molecules [271]. Specifically, they have carried out extensive CCSD(T)/CBS and dispersion-corrected DFT calculations in a CO₂/2-methylpyridine (the last with formula C₆H₇N) system. Stabilization of this complex occurs through an electron donor (2-methylpyridine)-electron acceptor (CO₂) mechanism and the attractive forces between oxygen and hydrogen atoms. The authors of work [271] show that in order to reproduce the E_{bind} gold-standard obtained with the CCSD(T)/CBS method (i.e., -0.14 eV), both electronic long-range exchange and correlations must be taken into account simultaneously. According to Mo’s calculations, BLYP-D3 is among the PBE-D3, BP86-D3, and TPSS-D3 methods (see Sec. III E) the one performing the best (i.e., providing a binding energy of -0.13 eV).

Conclusions.- The CO₂/2-methylpyridine complex is therefore a representative example of a system in which, despite of its reduced length, both van der Waals interactions and electronic long-range exchange are simultaneously important. Also, we note that “low-cost” dispersion-corrected DFT schemes like the BLYP-D3 one [173] appear to work remarkably well in this system. Indeed, it would be extremely interesting to check whether the adsorption of CO₂ (and H₂) molecules in alike cluster systems could be described correctly also with this last type of computationally cost-effective approaches.

The accuracy of standard and hybrid DFT functionals in describing the interactions of CO₂ molecules with Ca-decorated graphene has been recently assessed by Cazorla *et al.* [272]. In Cazorla’s work, a comparative study between DFT and MP2 calculations is presented by following an original recipe: instead of adopting the customary strategy of steadily increasing the size of polycyclic aromatic hydrocarbon (PAH) molecules, the concentration of Ca dopants in anthracene (i.e., C₁₄H₁₀, a relatively small PAH) is tuned so as to mimic the partial density of electronic valence states in Ca-decorated graphene (see Fig. 7a). The reason for doing that is to constrain the size of the cluster system where to carry out the MP2 calculations as much as possible, while still reproducing the main electronic orbital mechanisms occurring in the targeted extended material. In this way, the appearance of artificial electronic transitions upon gas-loading are prevented in the model cluster system (e.g., see work [220]). Cazorla’s results show that all considered DFT flavors predict equilibrium structures which are very similar to that obtained with the MP2 method, and energetically favourable CO₂ binding (see Figs. 7b-c). Nevertheless, the differences between hybrid DFT and MP2 energy estimations amount to ~ 0.4 eV, and between standard DFT and MP2 to $1.0 - 2.0$ eV, with DFT methods providing always the strongest binding. The origins of the observed hybrid DFT and MP2 numerical discrepancies (see Fig. 7c) are rationalized in terms of residual self-

interaction errors [272]. The amount of charge transferred between the gas molecules and $\text{Ca-C}_{14}\text{H}_{10}$ turns out to be the same when computed with either hybrid DFT or MP2 methods, and long-range dispersion interactions appear to be secondary in the present system (see Table 1 in work [272]). Cazorla *et al.* therefore conclude that the strength of the resulting electrostatic interactions, which are dominant, must be equal in the two compared cases. On the other side, LDA and PBE standard functionals overestimate the transfer of charge to the CO_2 molecule by 30 – 40% [272]. In light of those outcomes, the use of hybrid DFT functionals is recommended over that of local and semilocal approaches for investigation of the gas-uptake properties of AEM-decorated carbon GAM.

Conclusions.- Cazorla’s prescription for choosing a reduced cluster system in which to undertake quantum chemistry calculations may be useful for optimizing the computational expense associated to DFT benchmark tests. Also, for justifying the subsequent generalization of the attained conclusions to extended materials [272]. Nevertheless, only few selected electronic features of the targeted system (e.g., partial density of electronic states around the Fermi energy level) can be reproduced at a time by playing with doping strategies, and probably only at a qualitative level. In this context, recent methodological progress achieved in the resolution of the so-called “inverse band structure-problem of finding an atomic configuration with given electronic properties” problem [273, 274] (e.g., genetic algorithm searches), could be useful. In particular, those techniques could be applied to the design of model cluster systems that were replicas of the targeted extended GAM in terms of the electronic structure. In that case, besides the chemical stoichiometry, the atomic structure and shape of the simulation cell could be varied until finding a suitable system in which to perform all the calculations. (Of course, electronic long-range exchange and correlation corrections should be added somehow afterwards; this could be achieved, for instance, by carrying out additional calculations in both periodic and cluster systems with an adequate first-principles method.) We speculate that with such an original effective approach it could be possible to address important benchmark controversies affecting the performance of DFT methods in GAM modeling (e.g., those explained in the present and previous sections), while avoiding the computational burden and bias introduced by the finite size of model cluster systems.

2. MOF

The interplay between open-metal site MOF and CO_2 molecules is dominated by dispersion interactions, which represent about the 40 – 60 % of the total gas adsorption energy [275, 276]. Besides dispersion, electrostatic and orbital interactions are also important in shaping the gas

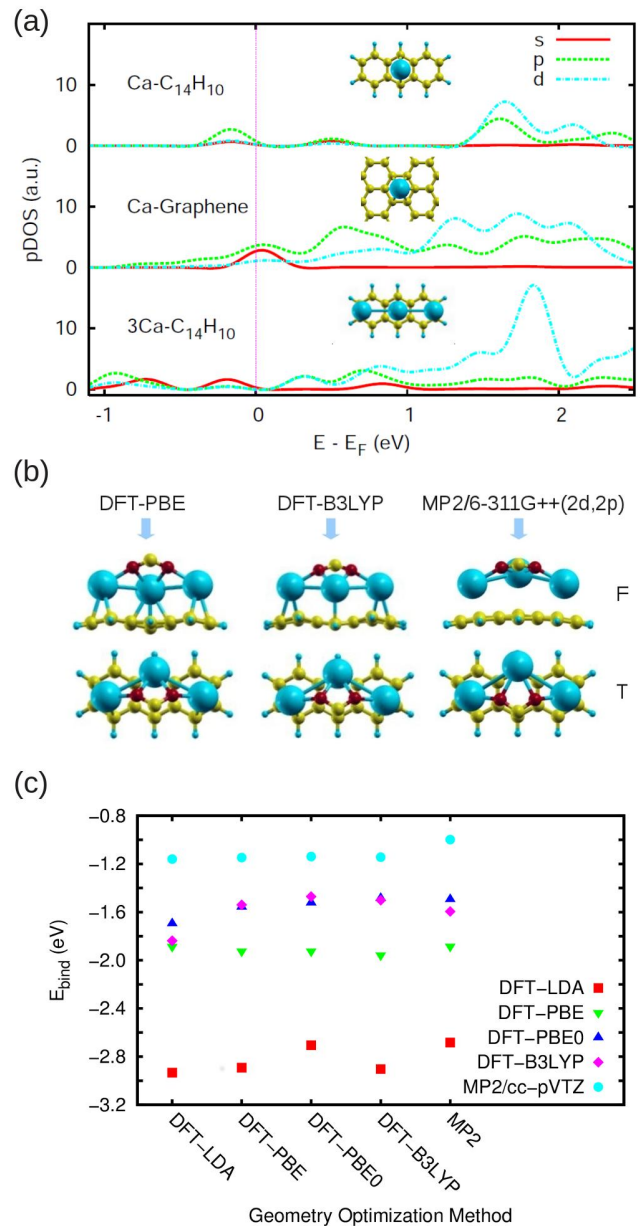


FIG. 7. (a) Partial density of electronic states calculated in Ca-anthracene, 3Ca-anthracene, and Ca-decorated graphene using DFT-PBE. (b) Equilibrium structures obtained for the adsorption of CO_2 in 3Ca-anthracene using DFT and MP2 methods. (c) Adsorption energies for CO_2 in 3Ca-anthracene obtained with different geometry optimization and total energy methods. (Figure adapted from work [272]).

affinity of MOF. In particular, puntual charges localized in the unsaturated metal sites polarize the CO_2 molecules inducing an electric dipole and a bend distortion in them [275, 277–279]. When low-energy empty d -levels are present a forward donation of electrons from CO_2 to the metal atoms occurs, which tends to increase the electrostatic contribution to the gas binding [275, 278, 280]. This last effect is particularly important in MOF-74 and

Work	MOF – type	DFT flavour	E_{bind}	ΔH	ΔH^{exp}
[277]	Mg – MOF74	PBE	−0.230	−0.189	−0.415
		PBE + D2	−0.439	−0.399	
		vdW – DF	−0.460	−0.420	
		vdW – DF2	−0.428	−0.388	
		vdW – PBE	−0.644	−0.604	
		vdW – optB88	−0.557	−0.517	
		vdW – C09 _x	−0.580	−0.540	
[13]					
[283]	Mg – DOBDC	LDA	−0.542	−0.531	−0.458 ± 0.048
		PBE	−0.228	−0.209	
		DFT – D2	−0.450	−0.411	
		vdW – DF	−0.528	−0.490	
		vdW – DF2	−0.500	−0.479	
		vdW – optB86b	−0.582	−0.559	
		vdW – optB88	−0.575	−0.547	
		vdW – optPBE	−0.608	−0.593	
		B3LYP + D	−0.430	−0.393	
		MP2 : B3LYP + D	−0.480	−0.443	
[284]					
[283]					
[283]	Ni – DOBDC	PBE	−0.124	−0.091	−0.410 ± 0.016
		DFT – D2	−0.361	−0.317	
		vdW – DF	−0.428	−0.392	
		vdW – DF2	−0.405	−0.358	
		vdW – optB86b	−0.504	−0.473	
		vdW – optB88	−0.496	−0.447	
		vdW – optPBE	−0.516	−0.483	
		B3LYP + D	−0.403	−0.368	
		MP2 : B3LYP + D	−0.455	−0.420	
[283]	Co – DOBDC	LDA	−0.408	−0.379	−0.370 ± 0.020
		PBE	−0.100	−0.086	
		DFT – D2	−0.322	−0.301	
		vdW – DF	−0.407	−0.386	
		vdW – DF2	−0.375	−0.337	
		vdW – optB86b	−0.455	−0.419	
		vdW – optB88	−0.452	−0.414	
		vdW – optPBE	−0.477	−0.453	
[283]	Cu – HKUST	LDA	−0.326	−0.317	−0.246 ± 0.085
		PBE	−0.092	−0.097	
		DFT – D2	−0.233	−0.192	
		vdW – DF	−0.283	−0.241	
		vdW – DF2	−0.264	−0.223	
		vdW – optB86b	−0.305	−0.263	
		vdW – optPBE	−0.329	−0.287	

TABLE VI. CO₂-MOF binding energies, E_{bind} , and heats of adsorption ($T = 300$ K), ΔH , calculated with different DFT exchange-correlation functionals. vdW-optB86b, vdW-optB88, and vdW-optPBE represent variants of the original vdW-DF and vdW-DF2 nonlocal functionals [176, 180] due to Klimeš and co-workers [181]. The vdW-C09_x variant is due to Cooper [182], and the vdW-PBE one is based on the PBE exchange functional [157] (see Sec. III E). Experimental values, ΔH^{exp} , correspond to measured heats of adsorption, and all energies are given in units of eV per molecule.

BTT species (see Sec. II C) containing Ti and V open-metal sites, where the σ^* antibonding state that results from the hybridization of oxygen CO_2 lone pairs and metal d_z^2 orbitals remains unoccupied [280]. In the case of heavily loaded MOF, quadrupolar CO_2 - CO_2 interactions turn out to be also very important.

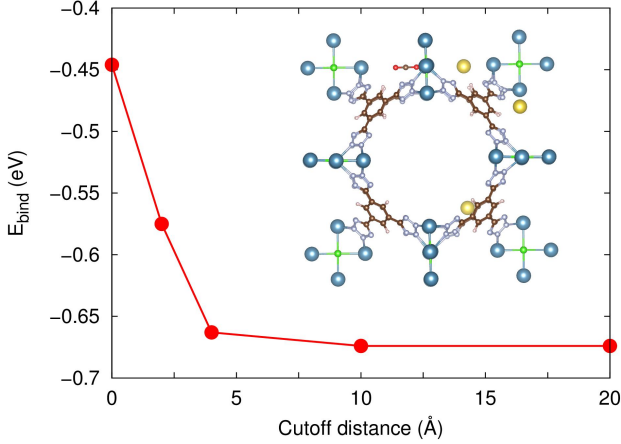


FIG. 8. Binding energy of a CO_2 molecule on Ca-BTT computed with the PBE+D2 approach, expressed as a function of the cutoff distance for the pairwise corrections (adapted from Ref. [277]). The CO_2 -MOF system in which calculations are performed is represented also in the figure.

Next, we review recent DFT benchmarking works done on the screening of MOF for applications in CO_2 capture and sequestration. Due to the crucial relevance of long-range interactions in CO_2 -MOF systems, we disregard here computational studies considering small organic molecules as model GAM (see, for instance, articles [281, 282] where the CO_2 -pyridine and CO_2 -benzene interactions are investigated) since proper convergence of long-range dispersion forces is achieved within distances of at least ~ 10 Å. This fact is illustrated in Fig. 8, which has been adapted from work [277], where the DFT binding energy of a CO_2 molecule on a MOF containing Ca open metal sites is represented as a function of the cutoff distance that is employed in the calculation of the dispersion interactions.

In Table VI, we enclose the results of gas binding energy and enthalpy of adsorption, ΔH , calculations performed by Poloni *et al.* [277] and Rana *et al.* [283] in different MOF, using standard and dispersion corrected DFT functionals. For present benchmarking purposes, comparisons with respect to quantum chemistry calculations performed in cluster-size model systems may result not meaningful because of the convergence reasons explained above, and thus the DFT outcomes are compared with experimental heats of adsorption. Enthalpies of adsorption at ambient temperature can be estimated with the formula $\Delta H = E_{\text{bind}} + \Delta E_{\text{ZPE}} + \Delta E_{\text{TE}}$. Here, ΔE_{ZPE} and ΔE_{TE} represent the zero-point energy (i.e., $E_{\text{ZPE}} = \sum_i \hbar \omega_i / 2$, $\{\omega_i\}$ being the corresponding vibrational phonon frequencies) and the thermal energy (i.e.,

$E_{\text{TE}} = E_{\text{vib}} + E_{\text{rot}} + E_{\text{transl}} + k_B T$ for the CO_2 gas phase -where $k_B T$ accounts for the energy of an ideal gas-, and $E_{\text{TE}} = E_{\text{vib}}$ for the framework with and without the adsorbate) differences, respectively, between the joint and disjoint CO_2 -MOF systems.

Upon comparison of the computed and measured ΔH values shown in Table VI, we can draw the following two conclusions: first, standard DFT methods are far from reproducing the experimental heat of adsorption trends, with LDA (PBE) presenting large underestimation (overestimation) bias; and second, among the two families of considered dispersion corrected approaches, i.e., semiempirical Grimme's and vdW- X (where X indicates the choice of the E_x^{GGA} functional -see Sec. III E-), the latter always provides the better agreement with respect to experiments (in particular, the vdW-DF and vdW-DF2 variants show null $\Delta H - \Delta H^{\text{exp}}$ discrepancies within the numerical uncertainties in most of the cases). It is worth noticing that the value of the ΔE_{ZPE} and ΔE_{TE} differences generally amount to less than ~ 50 meV, hence the major contribution to ΔH comes from the E_{bind} term. Also we note that the structural traits predicted in CO_2 -MOF systems with vdW- X methods, not shown here, present overall good agreement with the experiments.

In Table VI, we also include the ΔH results obtained by Valenzano *et al.* [284] with an hybrid MP2:B3LYP-D approach [285, 286]. In that scheme, MP2 calculations are carried out first in a cluster model system representing the adsorption site, and a long-range correction is added afterwards. The long-range correction is defined as the B3LYP-D energy difference between the extended and model cluster systems. (The MP2:B3LYP-D method can be likewise understood as starting from a B3LYP-D calculation for the full periodic structure and adding a high-level correction for the adsorption site.) Valenzano's MP2:B3LYP-D results obtained in the Mg- and Ni-DOBDC systems actually are in the same excellent agreement with experimental data than found with the vdW-DF and vdW-DF2 methods (i.e., null $\Delta H - \Delta H^{\text{exp}}$ discrepancies within the numerical uncertainties). Also, they represent an improvement with respect to primary B3LYP-D calculations [284]. On one hand, Valenzano's MP2:B3LYP-D work comes to reinforce the accuracy of vdW-DF methods in describing the gas uptake properties of MOF. On the other hand, it demonstrates the reliability and efficiency of the intuitive MP2:B3LYP-D approach for undertaking benchmark and GAM design studies.

Conclusions. - In light of the compiled results and analysis, it can be concluded that the use of standard DFT functionals must be avoided in the study of the CO_2 adsorption features of MOF. Meanwhile, the suite of vdW-DF methods currently represent the best choice for carrying out computational studies of such a type, both in terms of computational expense and reliability. In this regard, we would like to mention that in order to complete our knowledge of the general performance of DFT methods in the simulation of CO_2 -MOF systems it will be

highly desirable to consider meta-GGA functionals (e.g., M05-2X and M06-2X) in prospective studies. Also, it would be very interesting to perform advanced RPA-DFT and QMC benchmark calculations in those same systems for complementing the comparisons reported against experiments, and determining more precisely the role of the different energy contributions to the binding of molecules (e.g., many-body dispersion effects). Meanwhile, merging quantum chemistry methods (e.g., MP2) with periodic DFT simulations that incorporate long-range dispersion interactions, appears to be an effective strategy for calculating accurate binding energies in situations where the selected cluster and extended systems are physically alike.

V. DISCUSSION AND PROSPECTIVE WORK

From all the results and explanations presented in Sec. IV it can be concluded that standard DFT methods (i.e., LDA and GGA) generally provide results on the fixation of H_2 and CO_2 molecules in CN and MOF that are correct only at the qualitative level. Actually, in the sole analyzed case of hydrogen binding to chemically functionalized MOF coherent agreement between DFT-GGA results and highly accurate quantum chemistry calculations has been reported by several authors (see Sec. IV A 2). However, in that particular case full consistency between DFT results obtained in cluster size and periodic H_2 -MOF systems is still lacking, and further investigations are required for determining the precise role of dispersion interactions. Therefore, our general recommendation is to avoid using standard DFT methods in first-principles modeling of H_2 -storage and CCS materials when pursuing accurate binding energies and geometries. In stark contrast to this our advice, most of the computational studies published to date on gas-adsorption topics have relied heavily on the outcomes of DFT-LDA and DFT-GGA simulations (i.e., about the 80–60 % of them in the last 14 years). In Figs. 9 and 10, we show an estimation of the total number of DFT works reported in the areas of H_2 storage and CCS GAM modeling, classified according to the employed DFT functional and publication date.

In the case of hydrogen storage (see Fig. 9), we appreciate an important recent decline in the relative number of modeling studies performed with LDA and GGA functionals, as compared to the trend observed during the first decade of the present century (i.e., a decrease of the ~ 20 %). On the other side, the relative number of DFT works based on dispersion corrected schemes has increased significantly over the same period of time (i.e., from ~ 1 % to ~ 10 %). This last datum reflects, on one hand, the improved feasibility of electronic band structure methods incorporating van der Waals interactions (and the increasing availability through commercial packages) and, on the other, the awareness of the importance of this type of interactions within the community

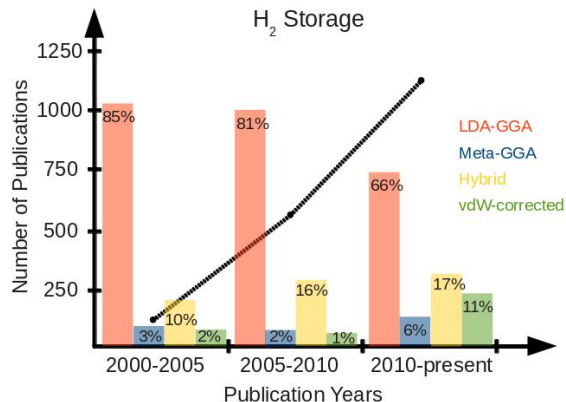


FIG. 9. Number of DFT-based “ H_2 storage” articles published from 2000 onwards, classified according to the employed E_{xc} approximation (our estimation relies on data extracted from the “Web of Knowledge”, December 2014). The solid dots represent the total number of works published in different years intervals, and the boxes the percentage corresponding to each DFT variant.

of materials scientists. Also, we notice that the popularity of hybrid and meta-GGA functionals have grown considerably within the last ten years. Nevertheless, all these trends refer to percentages and the truth is that, since the total number of published articles has grown almost linearly since year 2000, the total number of computational works that are prone to revision (i.e., those performed with standard DFT methods) has actually increased during the last years.

As for the modeling of CCS GAM (see Fig. 10), we also acknowledge a steady increase in the total number of published works and a significant recession in the percentage of recent LDA and GGA studies (i.e., a decrease from ~ 60 % to ~ 40 % in the last four years). Meanwhile, the number of dispersion corrected DFT works has increased remarkably in the last years, reaching a maximum peak of 25 % recently, while the use of hybrid functionals has been maintained more or less constant around 30 %. Also, meta-GGA functionals are becoming increasingly more popular although these are still the least preferred among all the considered DFT variants.

The ultimate DFT tendencies revealed in both H_2 storage and CCS GAM modeling fields are quite similar, namely there is a firm surge in the use of hybrid and dispersion corrected approaches in detriment to those of LDA and GGA. This fact shows that the outcomes of complex DFT benchmark studies are being assimilated progressively by the community of materials scientists specialized in GAM applications. In spite of this positive conclusion, the total number of recent GAM design works that still rely exclusively on LDA and GGA calculations is, in our opinion, unjustifiably too large.

In the Introduction section of this review we commented on the two main threats that customary DFT

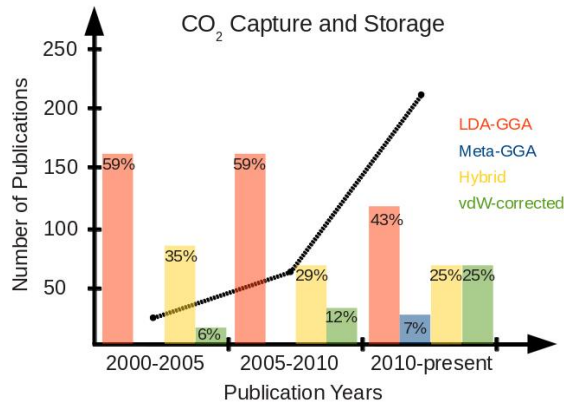


FIG. 10. Number of DFT-based “Carbon capture and storage” articles published from 2000 onwards, classified according to the employed E_{sc} approximation (our estimation relies on data extracted from the “Web of Knowledge”, December 2014). The solid dots represent the total number of works published in different years intervals, and the boxes the percentage corresponding to each DFT variant.

approaches pose to the design of GAM, namely the difficulties in (i) accounting simultaneously for the long range electron-electron exchange and correlations, both of which are omnipresent in gas-adsorption phenomena, and (ii) reproducing many-body energy effects and Coulomb screening in extended systems.

Regarding issue (i), we have demonstrated in Sec. IV that good agreement with respect to quantum chemistry calculations and experimental data is achieved when well-balanced exchange-correlation functionals are employed that include van der Waals interactions, on one hand, and correct to some extent for the inherent electron self-interaction errors, on the other. This is the case, for instance, of the mixed BLYP-D3 method which in the CO_2 /2-methylpyridine system has been shown to perform at the same level of accuracy than CCSD(T)/CBS (see Sec. IV B 1 and work [271]). Also, the so-called ω B97X-D approach, based on a range-separated hybrid and dispersion corrected DFT functional (see Sec. III D), has been shown to reproduce correctly the binding energy trends measured for H_2 molecules on metal-BTT complexes (see Sec. IV A 2 and work [250]). We consequently argue that the *safest* options for undertaking first-principles computational work on gas-adsorption applications and the design of GAM are to use DFT functionals which incorporate, either in an exact or approximate way, long range electron-electron exchange and correlations. The performance of these “full long range corrected” (FLRC) DFT functionals has been tested very recently by several authors in standard benchmark data sets, and very promising results have been attained in all the cases (e.g., see studies [168, 169, 171, 178]).

An interesting aspect of FLRC functionals is that these can be constructed in principle by taking any pure or long

range corrected hybrid DFT functional as a start, and subsequently adding the missing nonlocality of the correlation energy in the form of additional E_{xc} terms. Also, the degree of sophistication and computational expense associated to FLRC functionals can be chosen almost at wish by adopting simpler or more complex exchange-correlation correction schemes. For instance, a computationally inexpensive FLRC solution may consist in combining the semiempirical dispersion correction approach due to Grimme with any hybrid or meta DFT functional of one’s personal taste (e.g., the already employed ω B97X-D, TPSS-D3, M06-D3, and BLYP-D3 functionals). A superior FLRC blend, both in terms of accuracy and computational expense, could be achieved by considering full nonlocal functionals like vdW-DF or VV10 rather than semiempirical correlation correction schemes (see for instance work [178]). In conclusion, we strongly recommend to use FLRC functionals in future *ab initio* modeling of GAM and to analyze their performance comprehensively in prospective DFT benchmark studies.

Regarding the second customary DFT challenge (ii) mentioned above and explained in Sec. ID, many-body energy and Coulomb screening effects can vary considerably the polarizabilities, and consequently the forces, of gas molecules interacting with extended surfaces and other molecules [47, 195]. The RPA-DFT and DFT+MBD methods emerge as the two DFT variants which can deal efficiently with these types of many-body effects (see Sec. III F). In particular, the DFT+MBD method is very well suited for studying large periodic systems containing up to few hundreds of atoms [48–50]. Nevertheless, to the best of our knowledge, neither the RPA-DFT nor the DFT+MBD method has been applied yet to the simulation of hydrogen storage or carbon capture and sequestration problems, as shown by the lack of such studies in the comprehensive analysis presented in Sec. IV. Prospective RPA-DFT and DFT+MBD works targeting those GAM design areas are highly desirable for rationalizing further the causes underlying the discrepancies found between DFT-based and quantum chemistry methods [e.g., DMC and CCSD(T)], and in general for substantiating the role of many-body effects in the adsorption of gas molecules on atomically sparse environments. In fact, many-body DFT methods themselves present also a number of remaining challenges like it can be the derivation of an analytic expression for the calculation of atomic forces. (This ingredient is highly sought after for the realization of efficient geometry optimizations and molecular dynamics simulations.) Work on this and other directions have been already initiated [49, 50], thereby we expect that the application of many-body DFT methods will become routinary in the near future. We animate computational scientists to start considering these advanced computational techniques in their planned studies of GAM.

Concerning the generalization of DFT benchmark conclusions attained in cluster systems to realistic materials, we have presented evidence for a number of related issues

like are the omission of long range dispersion interactions and the disguise of electronic band structure effects (see, Secs. I E and IV). An effective way of getting rid of those potential drawbacks is to recover the translational invariance in the simulations and to perform all the required calculations in a same periodic system. This possibility naturally points to the suite of *exact* ground-state quantum Monte Carlo methods (e.g., diffusion Monte Carlo -DMC-) as one of the most promising approaches for undertaking benchmark studies on the performance of DFT. In fact, the formalism of Bloch functions is already firmly established within QMC [57, 58] and different implementations of this approach are available in several open-source packages (e.g., CASINO [59], QWALK [60], and QMCPACK [61]). Also, the computational cost of QMC calculations is orders of magnitude more favorable than those of other popular quantum chemistry methods. For these reasons, we envisage that QMC methods will play an increasingly more relevant role in prospective DFT benchmark studies of GAM. (Actually, the DMC method has already been applied to the study of metal hydrides [228, 229, 287] and metal oxides [288–290], two important families of materials within the context of hydrogen storage and carbon capture.) It is worth noticing, however, that QMC methods are neither exempt of some important technical problems. These are essentially related to the tediousness found in the computation of atomic forces [291, 292] and the correction of numerical bias introduced by the nodal surface approximation [58].

An alternative to using periodic quantum chemistry methods, which is computationally more feasible but also tentative, may consist in designing model cluster systems which mimic the electronic structure of targeted extended GAM (see Sec. IV B 1) and where all the hierarchical calculations are subsequently performed. In following this approach, one should correct somehow for the electronic long-range exchange and correlations in the final adsorption energies. This could be done *ad hoc* by carrying out additional calculations in both periodic and cluster systems with a suitable first-principles method (e.g., FLRC functionals like ω B97X-D and BLYP-D3). Such a proposed long-range correction scheme is very much on the spirit of hybrid DFT:QCM approaches, which have been demonstrated to be successful on the simulation of extended systems (e.g., see Sec. IV B 2 and works [285, 286]). The reliability of this alternative benchmark approach, however, has not been yet fully assessed hence further work on this direction is certainly needed before claiming any progress.

VI. GENERAL CONCLUSIONS

In this critical review, we have presented abundant evidence showing that both electronic long-range exchange and long-range correlations play a decisive role in the adsorption of H_2 and CO_2 molecules on carbon-based materials and MOF. Even in situations where the cal-

culated gas binding energies turn out to be large (i.e., $E_{\text{bind}} \geq 0.1$ eV), the same conclusion holds to be true. Consequently, DFT exchange-correlation functionals employed in the modeling of GAM must incorporate features which somehow correct for standard self-interaction errors and simultaneously reproduce dispersion forces. DFT E_{xc} functionals of this class include the brand-new BLYP-D3, ω B97X-D, and vdW-optB88 variants, to cite a few. Other similar “full long range corrected” functionals can be tailored in principle by combining hybrid and dispersion correction schemes of one’s personal taste, producing so a suite of *safe* DFT approaches which can range widely on versatility and computational expense.

As for standard DFT functionals (i.e., LDA and GGA), since these completely disregard electronic long-range exchange and correlations, we recommend not to use them in the modeling of GAM and simulation of gas adsorption phenomena in general. In some particular circumstances LDA and GGA approaches may provide the correct qualitative answers, however this is likely to occur fortuitously as a result of large error cancellations. Regrettably, current trends realized in modeling of GAM show that the use of LDA and GGA functionals is still quite widespread. We expect to motivate a change on this tendency with the present critical review. Also, we appeal to bring into new examination reported standard DFT predictions on GAM which are in conflict with observations.

Concerning prospective DFT work, we animate researchers to consider the RPA-DFT and DFT+MBD methods in future studies of H_2 storage and carbon capture materials. The reason for this is to substantiate with precision the role of many-body energy and Coulomb screening effects on the estimation of gas binding energies and equilibrium geometries. This is a completely new direction to take in modeling of GAM and, despite that the applicability of many-body DFT-based approaches remains yet limited, we believe that it will help in understanding further the origins of the discrepancies found between DFT and quantum chemistry results.

Finally, we recommend to be cautious in generalizing the conclusions of benchmark studies performed in model cluster systems to realistic GAM. In fact, the density of electronic states around the Fermi level and the HOMO and LUMO orbitals in chemically similar cluster and extended systems, even when considering medium size model complexes, can be very different. Those circumstances easily can translate into completely different gas-GAM governing interactions. Also, electronic long-range interactions present in extended materials generally turn out to be disguised in model cluster systems. The safest strategy for avoiding these potential scaling problems is to consider quantum chemistry methods which, alike to DFT, can handle the simulation of periodic systems. In this context, quantum Monte Carlo emerge as one the most effective suite of *exact* ground-state methods for computation of gold-standard benchmarks in GAM.

ACKNOWLEDGMENTS

This research was supported under the Australian Research Council's Future Fellowship funding scheme

(project number RG134363 and RG151175). The author would like to thank S. A. Shevlin for useful discussions on the organization of this review and for help in preparing Fig. 1.

-
- [1] L. Dai, D. W. Chang, J. B. Baek, and W. Lu, *Small* **8**, 1130 (2012).
 - [2] F. Bonaccorso, Z. Sun, T. Hasan, and A. C. Ferrari, *Nat. Photonics* **4**, 611 (2010).
 - [3] F. Yavari and N. Koratkar, *J. Phys. Chem. Lett.* **3**, 1746 (2012).
 - [4] G. Zhao, T. Wen, C. Chen, and X. Wang, *RSC Advances* **2**, 9286 (2012).
 - [5] N. G. Sahoo, Y. Pan, L. Li, and S. H. Chan, *Adv. Mater.* **24**, 4203 (2012).
 - [6] J. L. Mendoza-Cortes, W. A. Goddard III, H. Furukawa, O. M. Yaghi, *J. Phys. Chem. Lett.* **3**, 2671 (2012).
 - [7] A. M. Fracaroli, H. Furukawa, M. Suzuki, M. Dodd, S. Okajima, F. Gándara, J. A. Reimer, and O. M. Yaghi, *J. Am. Chem. Soc.* **136**, 8863 (2014).
 - [8] H. Furukawa and O. M. Yaghi, *J. Am. Chem. Soc.* **131**, 8875 (2009).
 - [9] D. P. Broom and K. M. Thomas, *MRS Bulletin* **38**, 412 (2013).
 - [10] S. Urbonaite, J. M. Juarez-Galan, J. Leis, F. Rodriguez-Reinoso and G. Svensson, *Microporous Mesoporous Mater.* **113**, 14 (2008).
 - [11] D. J. Tranchemontagne, K. S. Park, H. Furukawa, J. Eckert, C. B. Knobler, O. M. Yaghi, *J. Phys. Chem. C* **116**, 13143 (2012).
 - [12] Y. Yürüm, A. Taralp, and T. N. Veziroglu, *Int. J. Hydrog. Ener.* **34**, 3784 (2009).
 - [13] P. D. C. Dietzel, V. Besikiotis, and R. Blom, *J. Mat. Chem.* **19**, 7362 (2009).
 - [14] R. Kumar, V. M. Suresh, T. K. Maji, and C. N. R. Rao, *Chem. Commun.* **50**, 2015 (2014).
 - [15] J. M. Simmons, H. Wu, W. Zhou, and T. Yildirim, *Energy Environ. Sci.* **4**, 2177 (2011).
 - [16] US Department of Energy, *DOE Targets for Onboard Hydrogen Storage Systems for Light-Duty Vehicles* (2011), <http://www1.eere.energy.gov/hydrogenandfuelcells/>
 - [17] S. A. Rackley, *Carbon Capture and Storage*, Elsevier (2010).
 - [18] R. E. Hester, R. M. Harrison, *Carbon Capture: Sequestration and Storage*, RSC Pub (2010).
 - [19] D. Frenkel and B. Smit, *Understanding Molecular Simulation: From Algorithms to Applications*, Academic Press (2001).
 - [20] A. I. Skoulidas, *J. Am. Chem. Soc.* **126**, 1356 (2004).
 - [21] Z. Xiang, D. Cao, J. Lao, W. Wang, and D. P. Broom, *Energy Environ. Sci.* **3**, 1469 (2010).
 - [22] A. Battisti, S. Taioli, and G. Garberoglio, *Microporous and Mesoporous Mater.* **143**, 46 (2011).
 - [23] G. Garberoglio and S. Taioli, *Microporous Mesoporous Mater.* **163**, 215 (2012).
 - [24] G. Garberoglio, N. M. Pugno, and S. Taioli, *J. Phys. Chem. C* **119**, 1980 (2015).
 - [25] M. C. Gordillo and J. Boronat, *Phys. Rev. B* **84**, 033406 (2011).
 - [26] C. Cazorla and J. Boronat, *Phys. Rev. B* **88**, 224501 (2013).
 - [27] C. Carbonell, F. de Soto, C. Cazorla, J. Boronat, and M. C. Gordillo, *J. Low Temp. Phys.* **171**, 619 (2013).
 - [28] M. C. Gordillo, C. Cazorla, and J. Boronat, *Phys. Rev. B* **83**, 121406(R) (2011).
 - [29] G. Csányi, T. Albaret, M. C. Payne, and A. de Vita, *Phys. Rev. Lett.* **93**, 175503 (2004).
 - [30] A. Dzubak, L. Lin, J. Kim, J. A. Swisher, R. Poloni, S. N. Maximoff, B. Smit and L. Gagliardi, *Nature Chem.* **4**, 810 (2012).
 - [31] D. Vanderbilt, *Phys. Rev. B* **41**, 7892(R) (1990).
 - [32] N. Troullier and J. L. Martins, *Phys. Rev. B* **43**, 1993 (1991).
 - [33] P. E. Blöchl, *Phys. Rev. B* **50**, 17953 (1994).
 - [34] O. K. Andersen, *Phys. Rev. B* **12**, 3060 (1975).
 - [35] J. P. Perdew and A. Zunger, *Phys. Rev. B* **23**, 5048 (1981).
 - [36] C. Lee, W. Yang, and R. G. Parr, *Phys. Rev. B* **37**, 785 (1988).
 - [37] S. Patchkovskii and T. J. Ziegler, *J. Chem. Phys.* **116**, 7806 (2002).
 - [38] A. J. Cohen, P. Mori-Sánchez, and W. Yong, *Chem. Rev.* **112**, 289 (2011).
 - [39] K. Johnston, J. Kleis, B. I. Lundqvist, and R. M. Nieminen, *Phys. Rev. B* **77**, 121404(R) (2008).
 - [40] S. N. Steinmann, C. Piemontesi, A. Delachat, and C. Corminboeuf, *J. Chem. Theory Comput.* **8**, 1629 (2012).
 - [41] A. J. Misquitta, J. Spencer, A. J. Stone, and A. Alavi, *Phys. Rev. B* **82**, 075312 (2010).
 - [42] A. Tkatchenko, D. Alfè, and K. S. Kim, *J. Chem. Theory Comput.* **8**, 4317 (2012).
 - [43] V. V. Gobre and A. Tkatchenko, *Nature Comm.* **4**, 2341 (2013).
 - [44] J. F. Dobson, A. White, and A. Rubio, *Phys. Rev. Lett.* **96**, 073201 (2006).
 - [45] J. G. Ángyán, R. Liu, J. Toulouse, and G. Jansen, *J. Chem. Theory Comput.* **7**, 3116 (2011).
 - [46] A. Hesselmann, *Phys. Rev. A* **85**, 012517 (2012).
 - [47] V. G. Ruiz, W. Liu, E. Zojer, M. Scheffler, and A. Tkatchenko, *Phys. Rev. Lett.* **108**, 146103 (2012).
 - [48] A. Tkatchenko, R. A. DiStasio Jr, R. Car, and M. Scheffler, *Phys. Rev. Lett.* **108**, 236402 (2012).
 - [49] A. Ambrosetti, A. M. Reilly, R. A. DiStasio Jr, and A. Tkatchenko, *J. Chem. Phys.* **140**, 18A508 (2014).
 - [50] R. A. DiStasio Jr, V. V. Gobre, and A. Tkatchenko, *J. Phys.:Condens. Matt.* **26**, 213202 (2014).
 - [51] F. Manby in *Accurate Condensed-Phase Quantum Chemistry*, CRC Press (2010).
 - [52] C. Pisani and R. Dovesi, *Int. J. Quantum Chem.* **17**, 501 (1980).
 - [53] R. Dovesi, C. Pisani, C. Roetti, and V. R. Saunders, *Phys. Rev. B* **28**, 5781 (1983).
 - [54] M. Causà, R. Dovesi, R. Orlando, C. Pisani, and V. R. Saunders, *J. Phys. Chem.* **92**, 909 (1988).

- [55] J. Ma, A. Michaelides, and D. Alfè, *J. Chem. Phys.* **134**, 134701 (2011).
- [56] D. G. A. Smith and K. Patkowski, *J. Chem. Theory Comput.* **9**, 370 (2013).
- [57] G. Rajagopal, R. J. Needs, A. James, S. D. Kenny, and W. M. C. Foulkes, *Phys. Rev. B* **51**, 10591 (1995).
- [58] W. M. C. Foulkes, L. Mitas, R. J. Needs, and G. Rajagopal, *Rev. Mod. Phys.* **73**, 33 (2001).
- [59] R. J. Needs, M. D. Towler, N. D. Drummond, and P. López Ríos, *J. Phys.:Condens. Matt.* **22**, 023201 (2010).
- [60] L. K. Wagner, M. Bajdich, and L. Mitas, *J. Comput. Phys.* **228**, 3390 (2009).
- [61] QMCPACK, <http://qmcpack.cmscc.org/>
- [62] K. P. Esler *et al.*, *J. Phys.:Conf. Ser.* **125**, 012057 (2008).
- [63] M. Marsman, A. Grüneis, J. Paier, and G. Kresse, *J. Chem. Phys.* **130**, 184103 (2009).
- [64] A. Grüneis, M. Marsman, and G. Kresse, *J. Chem. Phys.* **133**, 074107 (2010).
- [65] A. Grüneis, G. H. Booth, M. Marsman, J. Spencer, A. Alavi, and G. Kresse, *J. Chem. Theory Comput.* **7**, 2780 (2011).
- [66] G. H. Booth, A. Grüneis, G. Kresse, and A. Alavi, *Nature* **493**, 365 (2013).
- [67] B. Assfour, S. Leoni, S. Yurchenko, and G. Seifert, *Int. J. Hydrog. Ener.* **36**, 6005 (2011).
- [68] J. Lan, D. Cao, W. Wang, T. Ben, and G. Zhy, *J. Phys. Chem. Lett.* **1**, 978 (2010).
- [69] H. Fang, H. Demir, P. Kamakoti, and D. S. Sholl, *J. Mater. Chem. A* **2**, 274 (2014).
- [70] J. Lan, D. Cao, and B. Smith, *ACS Nano* **4**, 4225 (2010).
- [71] X. Feng, X. Dinq, and D. Jianq, *Chem. Soc. Rev.* **41**, 6010 (2012).
- [72] A. L. M. Reddy, A. E. Tanur, and G. C. Walker, *Int. J. Hydrog. Ener.* **35**, 4138 (2010).
- [73] Q. Weng, X. Wang, C. Zhi, Y. Bando, and D. Golberg, *ACS Nano* **7**, 1558 (2013).
- [74] Y. Lin and J. W. Connell, *Nanoscale*, **4**, 6908 (2012).
- [75] A. M. Seayad and D. M. Antonelli, *Adv. Mater.* **16**, 765 (2004).
- [76] S. A. Shevlin and Z. X. Guo, *Chem. Soc. Rev.* **38**, 211 (2009).
- [77] D. Cazorla-Amorós, J. P. Joly, A. Linares-Solano, A. Marcilla-Gomis, and C. Salinas-Martínez de Lecea, *J. Phys. Chem.* **95**, 6611 (1991).
- [78] C. C. Dean, J. Blamey, N. H. Florin, M. J. Al-Jeboori, P. S. Fennell, *Chem. Eng. Res. Des.* **89**, 836 (2011).
- [79] S. Wang, S. Yan, X. Ma, and J. Gong, *Energy Environ. Sci.* **4**, 3805 (2011).
- [80] S. Ramachandran, J.-H. Ha, and D. K. Kim, *Catal. Comm.* **8**, 1934 (2007).
- [81] S. A. Shevlin, C. Cazorla, and Z. X. Guo, *J. Phys. Chem. C* **116**, 13488 (2012).
- [82] S. A. Shevlin and Z. X. Guo, *J. Phys. Chem. C* **117**, 10883 (2013).
- [83] X. Sun, J. -Y. Hwang, and S. Shi, *J. Phys. Chem. C* **114**, 7178 (2010).
- [84] J. Gebhardt, F. Viñes, P. Bleiziffer, W. Hieringer, and A. Görling, *Phys. Chem. Chem. Phys.* **16**, 5382 (2014).
- [85] V. Bérubé, G. Radtke, M. Dresselhaus, and G. Chen, *Int. J. Ener. Res.* **31**, 637 (2007).
- [86] Y. Hu, O. A. Shenderova, Z. Hu, C. W. Padgett, and D. W. Brenner, *Rep. Prog. Phys.* **69**, 1847 (2006).
- [87] J. R. Li, Y. Ma, M. C. McCarthy, J. P. Sculley, J. Yu, H. Jeong, P. B. Balbuena, and H. Zhou, *Coord. Chem. Rev.* **255**, 1791 (2011).
- [88] S. Orimo, A. Züttel, L. Schlapbach, G. Majer, T. Fukunaga, H. Fujii, *J. All. Comp.* **356**, 716 (2003).
- [89] R. J. Kuppler, D. J. Timmons, Q. Fang, J. R. Li, T. A. Makal, M. D. Young, D. Yuan, D. Zhao, W. Zhuang, H. Zhou, *Coord. Chem. Rev.* **253**, 3042 (2009).
- [90] D. Tasis, N. Tagmatarchis, A. Bianco, and M. Prato, *Chem. Rev.* **106**, 1105 (2006).
- [91] A. Pakdel, C. Zhi, Y. Bando, T. Nakayama, and D. Golberg, *ACS Nano* **5**, 6507 (2011).
- [92] A. Nag, K. Raidongia, K. P. S. S. Hembram, R. Datta, U. V. Waghmare, and C. N. R. Rao, *ACS Nano* **4**, 1539 (2010).
- [93] N. Park, K. Choi, J. Hwang, D. W. Kim, D. O. Kim, and J. Ihm, *PNAS* **109**, 19893 (2012).
- [94] L. J. Murray, M. Dincă, and J. R. Long, *Chem. Soc. Rev.* **38**, 1294 (2009).
- [95] J. Yang, A. Sudik, C. Wolverton, and D. J. Siegel, *Chem. Soc. Rev.* **39**, 656 (2010).
- [96] D. M. D'Alessandro, B. Smit, and J. R. Long, *Angew. Chem. Int. Ed.* **49**, 6058 (2010).
- [97] A. Samanta, A. Zhao, G. K. H. Shimizu, P. Sarkar, and R. Gupta, *Ind. Eng. Chem. Res.* **51**, 1438 (2012).
- [98] S. Choi, J. H. Drese, and C. W. Jones, *ChemSusChem* **2**, 796 (2009).
- [99] R. C. Lochan and M. Head-Gordon, *Phys. Chem. Chem. Phys.* **8**, 1357 (2006).
- [100] <http://www1.eere.energy.gov/hydrogenandfuelcells/>.
- [101] S. Satyapal, J. Petrovic, C. Read, G. Thomas, and G. Ordaz, *Catal. Today* **120**, 246 (2007).
- [102] G. Garberoglio, A. I. Skoulidas, and J. K. Johnson, *J. Phys. Chem. B* **109**, 13094 (2005).
- [103] S. K. Bathia and A. L. Myers, *Langmuir* **22**, 1688 (2006).
- [104] A. Basile and A. Iulianelli, *Advances in Hydrogen Production, Storage and Distribution*, Woodhead Publishing, Cambridge (2014).
- [105] J. Li, T. Furuta, H. Goto, T. Ohashi, Y. Fujiwara, and S. Yip, *J. Chem. Phys.* **119**, 2376 (2003).
- [106] A. Bhattacharya, S. Bhattacharya, C. Majumder, and G. P. Das, *J. Phys. Chem. C* **114**, 10297 (2010).
- [107] A. Hamaed, H. V. Mai, T. K. A. Hoang, M. Trudeau, M. Antonelli, *J. Phys. Chem. C* **114**, 8651 (2010).
- [108] A. B. Phillips and B. S. Shivaram, *Phys. Rev. Lett.* **100**, 105505 (2008).
- [109] G. J. Kubas, *J. Organomet. Chem.* **635**, 37 (2001).
- [110] G. J. Kubas, *Chem. Rev.* **107**, 4152 (2007).
- [111] C. S. Tao *et al.*, *J. Phys. Chem. Lett.* **1**, 1060 (2010).
- [112] G. M. Psofogiannakis, G. E. Froudakis, *J. Am. Chem. Soc.* **131**, 15133 (2009).
- [113] G. M. Psofogiannakis, G. E. Froudakis, *Chem. Commun.* **47**, 7933 (2011).
- [114] Y. Li and R. T. Yang, *Langmuir* **23**, 12937 (2007).
- [115] T. Wang, Q. Zhang, B. Li, H. Chen, and L. Chen, *Int. J. Hydrog. Ener.* **37**, 5081 (2012).
- [116] D. Aaron and C. Tsouris, *Sep. Sci. Technol.* **40**, 321 (2005).
- [117] J. D. Gilchrist, *Extraction Metallurgy*, Pergamon Press, Oxford (1989).
- [118] C. Cazorla, S. A. Shevlin, and Z. X. Guo, *J. Phys. Chem. C* **115**, 10990 (2011).

- [119] J. W. G. Wilder, L. C. Venema, A. G. Rinzler, R. E. Smalley, and C. Dekker, *Nature* **391**, 59 (1998).
- [120] A. H. Castro Neto, F. Guinea, N. M. R. Peres, K. S. Novoselov, and A. K. Geim, *Rev. Mod. Phys.* **81**, 109 (2009).
- [121] M.-M. Rohmer, M. Bénard, C. Henriët, C. Bo, and J.-M. Poble, *J. Chem. Soc.: Chem. Commun.*, 1182 (1993).
- [122] M.-M. Rohmer, M. Bénard, C. Henriët, C. Bo, and J.-M. Poble, *J. Am. Chem. Soc.* **117**, 508 (1995).
- [123] M. S. Dresselhaus and G. Dresselhaus, *Adv. Phys.* **51**, 1 (2002).
- [124] N. Emery, C. Herold, and P. Lagrange, *J. Solid State Chem.* **178**, 2947 (2005).
- [125] M. Cobian and J. Iñiguez, *J. Phys.: Condens. Matter* **20**, 285212 (2008).
- [126] H. Lee, J. Ihm, M. L. Cohen, and S. G. Louie, *Nano Lett.* **10**, 793 (2010).
- [127] C. Cazorla, *Thin Solid Films* **518**, 6951 (2010).
- [128] A. V. Krashenninnikov and F. Banhart, *Nature Mat.* **6**, 723 (2007).
- [129] M. S. Dresselhaus, A. Jorio, M. Hofmann, G. Dresselhaus, and R. Saito, *Nano Lett.* **10**, 751 (2010).
- [130] M. Zhou, Y. Lu, C. Zhang, *et al.*, *Appl. Phys. Lett.* **97**, 103109 (2010).
- [131] D. Dutta, B. C. Wood, S. Y. Bhidé, K. G. Ayappa, and S. Narasimhan, *J. Phys. Chem. C* **118**, 7741 (2014).
- [132] S. A. Shevlin and Z. X. Guo, *J. Phys. Chem. C* **112**, 17456 (2008).
- [133] T. Yildirim and S. Ciraci, *Phys. Rev. Lett.* **94**, 175501 (2005).
- [134] C. Ataca, E. Aktürk, S. Ciraci, *Phys. Rev. B* **79**, 041406(R) (2009).
- [135] C. Cazorla, V. Rojas-Cervellera, and C. Rovira, *J. Mater. Chem.* **22**, 19684 (2012).
- [136] Q. Sun, Q. Wang, P. Jena, and Y. Kawazoe, *J. Am. Chem. Soc.* **127**, 145802 (2005).
- [137] S. Li and P. Jena, *Phys. Rev. Lett.* **97**, 209601 (2006).
- [138] C. Cazorla, S. A. Shevlin, and Z. X. Guo, *Phys. Rev. B* **82**, 155454 (2010).
- [139] M.-X. Wang, Q. Liu, Z.-F. Li, H.-F. Sun, E. A. Stach, and J. Xie, *J. Phys. Chem. Lett.* **4**, 1484 (2013).
- [140] F. Banhart, J. Kotakoski, and A. V. Krashenninnikov, *ACS Nano* **5**, 26 (2010).
- [141] H. Furukawa, K. E. Cordova, M. O’Keeffe, and O. M. Yaghi, *Science* **341**, 1230444 (2013).
- [142] S. S. Kaye and J. R. Long, *J. Am. Chem. Soc.* **130**, 806 (2008).
- [143] F. Schröder, D. Esken, M. Cokoja, M. W. E. van den Berg, O. I. Lebedev, G. V. Tendeloo, B. Walaszek, G. Buntkowsky, H.-H. Limbach, B. Chaudret, and R. A. Fischer, *J. Am. Chem. Soc.* **130**, 6119 (2008).
- [144] M. Dixit, T. A. Maark, K. Ghatak, R. Ahuja, and S. Pal, *J. Phys. Chem. C* **116**, 17336 (2012).
- [145] Y. E. Cheon and M. P. Suh, *Angew Chem. Int. Ed.* **48**, 2899 (2009).
- [146] D. W. Lim, J. W. Yoon, K. Y. Ryu, and M. P. Suh, *Angew. Chem.* **124**, 9952 (2012).
- [147] Jeon K.-J. *et al.*, *Nat. Mater.* **10**, 286 (2011).
- [148] W. Kohn and L. J. Sham, *Phys. Rev.* **140**, A1133 (1965).
- [149] L. J. Sham and W. Kohn, *Phys. Rev.* **145**, 561 (1966).
- [150] J. P. Perdew, *MRS Bulletin* **38**, 743 (2013).
- [151] J. Klimeš and A. Michaelides, *J. Chem. Phys.* **137**, 120901 (2012).
- [152] X. Ren, P. Rinke, C. Joas, and M. Scheffler, *J. Mater. Sci.* **47**, 7447 (2012).
- [153] J. F. Dobson and T. Gould, *J. Phys.: Condens. Matter* **24**, 073201 (2012).
- [154] S. N. Steinmann, Ph. D. thesis, École Polytechnique Fédérale de Lausanne, 2012.
- [155] D. M. Ceperley and B. I. Alder, *Phys. Rev. Lett.* **45**, 566 (1980).
- [156] J. P. Perdew, J. A. Chevary, S. H. Vosko, K. A. Jackson, M. R. Pederson, D. J. Singh, and C. Fiolhais, *Phys. Rev. B* **46**, 6671 (1992).
- [157] J. P. Perdew, K. Burke, and M. Ernzerhof, *Phys. Rev. Lett.* **77**, 3865 (1996).
- [158] J. Tao, J. P. Perdew, V. N. Staroverov, and G. E. Scuseria, *Phys. Rev. Lett.* **91**, 146401 (2003); J. P. Perdew, A. Ruzsinszky, G. I. Csonka, L. A. Constantin, and J. Sun, *Phys. Rev. Lett.* **103**, 026403 (2009).
- [159] J. Sun, B. Xiao, and A. Ruzsinszky, *J. Chem. Phys.* **137**, 051101 (2012); J. Sun, R. Haunschild, B. Xiao, I. W. Bulik, G. E. Scuseria, J. P. Perdew, *J. Chem. Phys.* **138**, 044113 (2013).
- [160] Y. Zhao, N. E. Schultz, and D. G. Truhlar, *J. Chem. Phys.* **123**, 161103 (2005); Y. Zhao, N. E. Schultz, and D. G. Truhlar, *J. Chem. Theor. Comput.* **2**, 364 (2006); Y. Zhao and D. G. Truhlar, *J. Phys. Chem. A* **110**, 13126 (2006).
- [161] Gaussian 09, Revision D.01, M. J. Frisch, G. W. Trucks, H. B. Schlegel, G. E. Scuseria, M. A. Robb, J. R. Cheeseman, G. Scalmani, V. Barone, B. Mennucci, G. A. Petersson, H. Nakatsuji, M. Caricato, X. Li, H. P. Hratchian, A. F. Izmaylov, J. Bloino, G. Zheng, J. L. Sonnenberg, M. Hada, M. Ehara, K. Toyota, R. Fukuda, J. Hasegawa, M. Ishida, T. Nakajima, Y. Honda, O. Kitao, H. Nakai, T. Vreven, J. A. Montgomery, Jr., J. E. Peralta, F. Ogliaro, M. Bearpark, J. J. Heyd, E. Brothers, K. N. Kudin, V. N. Staroverov, R. Kobayashi, J. Normand, K. Raghavachari, A. Rendell, J. C. Burant, S. S. Iyengar, J. Tomasi, M. Cossi, N. Rega, J. M. Millam, M. Klene, J. E. Knox, J. B. Cross, V. Bakken, C. Adamo, J. Jaramillo, R. Gomperts, R. E. Stratmann, O. Yazyev, A. J. Austin, R. Cammi, C. Pomelli, J. W. Ochterski, R. L. Martin, K. Morokuma, V. G. Zakrzewski, G. A. Voth, P. Salvador, J. J. Dannenberg, S. Dapprich, A. D. Daniels, Ö. Farkas, J. B. Foresman, J. V. Ortiz, J. Cioslowski, and D. J. Fox, Gaussian, Inc., Wallingford CT, 2009.
- [162] M. Valiev, E. J. Bylaska, N. Govind, K. Kowalski, T. P. Straatsma, H. J. J. van Dam, D. Wang, J. Nieplocha, E. Apra, T. L. Windus, and W. A. de Jong, *Comput. Phys. Commun.* **181**, 1477 (2010).
- [163] J. M. Soler, E. Artacho, J. D. Gale, A. García, J. Junquera, P. Ordejón, and D. Sánchez-Portal, *J. Phys.: Condens. Matter* **14**, 2745 (2002).
- [164] G. Kresse and J. Hafner, *Phys. Rev. B* **47**, 558 (1993); G. Kresse and J. Furthmüller, *Phys. Rev. B* **54**, 11169 (1996).
- [165] A. D. Becke, *J. Chem. Phys.* **98**, 5648 (1993); K. Kim and K. D. Jordan, *J. Phys. Chem.* **98**, 10089 (1994).
- [166] J. Heyd, G. E. Scuseria, and M. Ernzerhof, *J. Chem. Phys.* **118**, 8207 (2003).

- [167] J. P. Perdew, M. Ernzerhof, and K. Burke, *J. Chem. Phys.* **105**, 9982 (1996); M. Ernzerhof and G. E. Scuseria, *J. Chem. Phys.* **110**, 5029 (1999); C. Adamo and V. Barone, *J. Chem. Phys.* **110**, 6158 (1999).
- [168] J.-D. Chai and M. Head-Gordon, *Phys. Chem. Chem. Phys.* **10**, 6615 (2008).
- [169] Y.-S. Lin, G.-D. Li, S.-P. Mao, and J.-D. Chai, *J. Chem. Theory Comput.* **9**, 263 (2013).
- [170] T. Schwabe and S. Grimme, *Phys. Chem. Chem. Phys.* **9**, 3397 (2007).
- [171] N. Mardirossian and M. Head-Gordon, *Phys. Chem. Chem. Phys.* **16**, 9904 (2014).
- [172] S. Grimme, *J. Comput. Chem.* **25**, 1463 (2004); S. Grimme, *J. Comput. Chem.* **27**, 1787 (2006).
- [173] S. Grimme, J. Antony, S. Ehrlich, and H. Krieg, *J. Chem. Phys.* **132**, 154104 (2010).
- [174] A. Tkatchenko and M. Scheffler, *Phys. Rev. Lett.* **102**, 073005 (2009).
- [175] A. D. Becke, *J. Chem. Phys.* **122**, 064101 (2005); A. D. Becke and E. R. Johnson, *J. Chem. Phys.* **123**, 154101 (2005); A. D. Becke and E. R. Johnson, *J. Chem. Phys.* **127**, 154108 (2007).
- [176] M. Dion, H. Rydberg, E. Schröder, D. C. Langreth, and B. I. Lundqvist, *Phys. Rev. Lett.* **92**, 246401 (2004).
- [177] O. A. Vydrov and T. V. Voorhis, *J. Chem. Phys.* **133**, 244103 (2010).
- [178] O. A. Vydrov and T. V. Voorhis, *J. Chem. Theory Comput.* **8**, 1929 (2012).
- [179] R. Sabatini, T. Gorni, and S. Gironcoli, *Phys. Rev. B* **87**, 041108(R) (2013).
- [180] K. Lee, E. D. Murray, L. Kong, B. I. Lundqvist, and D. C. Langreth, *Phys. Rev. B* **82**, 081101 (2010).
- [181] J. Klimeš, D. R. Bowler, and A. Michaelides, *J. Phys.: Condens. Matter* **22**, 022201 (2010); J. Klimeš, D. R. Bowler, and A. Michaelides, *Phys. Rev. B* **83**, 195131 (2011); J. Carrasco, B. Santra, J. Klimeš, and A. Michaelides, *Phys. Rev. Lett.* **106**, 026101 (2011).
- [182] V. R. Cooper, *Phys. Rev. B* **81**, 161104(R) (2010).
- [183] G. Román-Pérez and J. M. Soler, *Phys. Rev. Lett.* **103**, 096102 (2009).
- [184] X. Ren, A. Tkatchenko, P. Rinke, and M. Scheffler, *Phys. Rev. Lett.* **106**, 153003 (2011).
- [185] S. L. Adler, *Phys. Rev.* **126**, 413 (1962).
- [186] N. Wiser, *Phys. Rev.* **129**, 62 (1963).
- [187] D. Lu, Y. Li, D. Rocca, and G. Galli, *Phys. Rev. Lett.* **102**, 206411 (2009).
- [188] H. Eshuis, J. Yarkony, and F. Furche, *J. Chem. Phys.* **132**, 234114 (2010).
- [189] H. Eshuis and F. Furche, *J. Chem. Phys. Lett.* **2**, 983 (2011).
- [190] H. Eshuis and F. Furche, *J. Chem. Phys.* **136**, 084105 (2012).
- [191] P. Umari, G. Stenuit, and S. Baroni, *Phys. Rev. B* **81**, 115104 (2010).
- [192] F. Furche, *Phys. Rev. B* **64**, 195120 (2001).
- [193] J. Harl and G. Kresse, *Phys. Rev. Lett.* **103**, 056401 (2010); J. Harl, L. Schimka, and G. Kresse, *Phys. Rev. B* **81**, 115126 (2010).
- [194] B. Xiao, J. Sun, A. Ruzsinszky, J. Feng, and J. P. Perdew, *Phys. Rev. B* **86**, 094109 (2012).
- [195] L. Schimka, J. Harl, A. Stroppa, A. Grüneis, M. Marsman, F. Mittendorfer, and G. Kresse, *Nature Mat.* **9**, 741 (2010).
- [196] G.-X. Zhang, A. Tkatchenko, J. Paier, H. Appel, and M. Scheffler, *Phys. Rev. Lett.* **107**, 245501 (2011).
- [197] X. Gonze, J.-M. Beuken, R. Caracas, F. Detraux, M. Fuchs, G.-M. Rignanese, L. Sindic, M. Verstraete, G. Zerah, F. Jollet, M. Torrent, A. Roy, M. Mikami, Ph. Ghosez, J.-Y. Raty, and D.C. Allan, *Comp. Mater. Sci.* **25**, 478 (2002).
- [198] G. te Velde, F. M. Bickelhaupt, E. J. Baerends, C. Fonseca Guerra, S. J. A. van Gisbergen, J. G. Snijders, and T. Ziegler, *J. Comp. Chem.* **22**, 931 (2001).
- [199] S. J. Clark, M. D. Segall, C. J. Pickard, P. J. Hasnip, M. I. J. Probert, K. Refson, and M. C. Payne, *Zeitschrift für Kristallographie* **220**, 5-6 (2005).
- [200] J. Hutter, M. Iannuzzi, F. Schiffmann, and J. VandeVondele, *WIREs Comput. Mol. Sci.* **4**, 15 (2014).
- [201] R. Dovesi, R. Orlando, A. Erba, C. M. Zicovich-Wilson, B. Civalieri, S. Casassa, L. Maschio, M. Ferrabone, M. De La Pierre, P. D'Arco, Y. Noel, M. Causa, M. Rerat, and B. Kirtman, *Int. J. Quantum Chem.* **114**, 1287 (2014).
- [202] M.F. Guest, I. J. Bush, H.J.J. van Dam, P. Sherwood, J.M.H. Thomas, J.H. van Lenthe, R.W.A. Havenith, and J. Kendrick, *Mol. Phys.* **103**, 719 (2005).
- [203] J. J. Mortensen, L. B. Hansen, and K. W. Jacobsen, *Phys. Rev. B* **71**, 035109 (2005).
- [204] H. -J. Werner, P. J. Knowles, G. Knizia, F. R. Manby, and M. Schütz, *WIREs Comput. Mol. Sci.*, **2**, 242 (2012).
- [205] P. Giannozzi, S. Baroni, N. Bonini, M. Calandra, R. Car, C. Cavazzoni, D. Ceresoli, G. L. Chiarotti, M. Cococcioni, I. Dabo, A. Dal Corso, S. de Gironcoli, S. Fabris, G. Fratesi, R. Gebauer, U. Gerstmann, C. Gougousis, A. Kokalj, M. Lazzeri, L. Martin-Samos, N. Marzari, F. Mauri, R. Mazzarello, S. Paolini, A. Pasquarello, L. Paulatto, C. Sbraccia, S. Scandolo, G. Sciauzero, A. P. Seitsonen, A. Smogunov, P. Umari, and R. M. Wentzcovitch, *J. Phys.: Condens. Matter*, **39**, 395502 (2009).
- [206] K. Schwarz, *J. Sol. Stat. Chem.* **176**, 319 (2003).
- [207] J. Kästner, H. M. Senn, S. Thiel, N. Otte, and W. Thiel, *J. Chem. Theory Comput.* **2**, 452 (2006).
- [208] S. Taioli, C. Cazorla, M. J. Gillan, and D. Alfè, *Phys. Rev. B* **75**, 214103 (2007).
- [209] C. Cazorla, M. J. Gillan, S. Taioli, and D. Alfè, *J. Chem. Phys.* **126**, 194502 (2007).
- [210] C. Cazorla, D. Alfè, and M. J. Gillan, *Phys. Rev. B* **85**, 064113 (2012).
- [211] W. Zhou, J. Zhou, J. Shen, C. Oujang, and S. Shi, *J. Phys. Chem. Solids* **73**, 245 (2012).
- [212] Z. M. Ao and F. M. Peeters, *Phys. Rev. B* **81**, 205406 (2010).
- [213] C.-H. Chen, T.-Y. Chung, C.-C. Shen, M.-S. Yu, C.-S. Ts, G.-N. Shi, C.-C. Huang, M.-D. Ger, and W.-L. Lee, *Int. J. Hydrog. Ener.* **38**, 3681 (2013).
- [214] W. G. Hong, B. H. Kim, S. M. Lee, H. Y. Yu, Y. J. Yun, Y. Yun, J. B. Lee, and H. J. Kim, *Int. J. Hydrog. Ener.* **37**, 7594 (2012).
- [215] C.-C. Huang, Y.-H. Li, Y.-W. Wang, and C.-H. Chen, *Int. J. Hydrog. Ener.* **38**, 3994 (2013).
- [216] H. Zhou, Z. Liu, J. Zhang, X. Yan, Y. Liu, and A. Yuan, *Int. J. Hydrog. Ener.* **39**, 2160 (2014).
- [217] J. Cha, S. Lim, C. H. Choi, M.-H. Cha, and N. Park, *Phys. Rev. Lett.* **103**, 216102 (2009).
- [218] Y. Ohk, Y.-H. Kim, and Y. Jung, *Phys. Rev. Lett.* **104**, 179601 (2010).

- [219] J. Cha, C. H. Choi, and N. Park, *Phys. Rev. Lett.* **104**, 179602 (2010).
- [220] J. Cha, C. H. Choi, and N. Park, *Chem. Phys. Lett.* **513**, 256 (2011).
- [221] O. Gunnarsson and R. O. Jones, *Phys. Rev. B* **31**, 7588 (1985).
- [222] M. Bajdich, R. A. Reboredo, and P. R. C. Kent, *Phys. Rev. B* **82**, 081405(R) (2011).
- [223] W. Purwanto, H. Krakauer, Y. Virgus, and S. Zhang, *J. Chem. Phys.* **135**, 164105 (2011).
- [224] V. Wang, H. Mizuseki, H. P. He, G. Chen, S. L. Zhang, and Y. Kawazoe, *Comp. Mater. Sci.* **55**, 180 (2012).
- [225] T. Hussain, B. Pathak, M. Ramzan, T. A. Maark, and R. Ahuja, *Appl. Phys. Lett.* **100**, 183902 (2012).
- [226] C. Li, J. Li, F. Wu, S.-S. Li, J.-B. Xia, and L.-W. Wang, *J. Phys. Chem. C* **115**, 23221 (2011).
- [227] J. Wong, S. Yadav, J. Tam, and C. V. Singh, *J. Appl. Phys.* **115**, 224301 (2014).
- [228] Z. Wu, M. D. Allendorf, and J. C. Grossman, *J. Am. Chem. Soc.* **131**, 13918 (2009).
- [229] S. Binnie, S. J. Nolan, N. D. Drummond, D. Alfè, N. L. Allan, F. R. Manby, and M. J. Gillan, *Phys. Rev. B* **82**, 165431 (2010).
- [230] L. K. Wagner, *Int. J. Quantum Chem.* **114**, 94 (2014).
- [231] A. Kuc, T. Heine, G. Seifert, and H. A. Duarte, *Theor. Chem. Account* **120**, 543 (2008).
- [232] A. Kuc, T. Heine, G. Seifert, and H. A. Duarte, *Chem. Eur. J.* **14**, 6597 (2008).
- [233] K. Sillar, A. Hofmann, and J. Sauer, *J. Am. Chem. Soc.* **131**, 4143 (2009).
- [234] J. Joo, H. Kim, and S. S. Han, *Phys. Chem. Chem. Phys.* **15**, 18822 (2013).
- [235] J. L. C. Rowsell and O. M. Yaghi, *Angew. Chem. Int. Ed.* **44**, 4670 (2005).
- [236] S. S. Han, J. L. Mendoza-Cortés, and W. A. Goddard III, *Chem. Soc. Rev.* **38**, 1460 (2009).
- [237] S. S. Han and W. A. Goddard III, *J. Phys. Chem. C* **112**, 13431 (2008).
- [238] R. C. Lochan, R. Z. Khaliullin, and M. Head-Gordon, *Inorg. Chem.* **47**, 4032 (2008).
- [239] W. Zhou, H. Wu, and T. Yildirim, *J. Am. Chem. Soc.* **130**, 15268 (2008).
- [240] Y. Y. Sun, Y.-H. Kim, and S. B. Zhang, *J. Am. Chem. Soc.* **129**, 12606 (2007).
- [241] R. M. Kumar, J. V. Sundar, and V. Subramanian, *Int. J. Hydrog. Ener.* **37**, 16070 (2012).
- [242] S. S. Han and W. A. Goddard III, *J. Am. Chem. Soc.* **129**, 8422 (2007).
- [243] E. Klontzas, A. Mavrandonakis, E. Tylianakis, and G. E. Froudakis, *Nano Lett.* **8**, 1572 (2008).
- [244] K. L. Mulfort and J. T. Hupp, *Inorg. Chem.* **47**, 7936 (2008).
- [245] Y. Y. Sun, K. Lee, Y.-H. Kim, and S. B. Zhang, *Appl. Phys. Lett.* **95**, 033109 (2009).
- [246] Y. Y. Sun, K. Lee, L. Wang, Y.-H. Kim, W. Chen, Z. Chen, and S. B. Zhang, *Phys. Rev. B* **82**, 073401 (2010).
- [247] M. Dixit, T. A. Maark, and S. Pal, *Int. J. Hydrog. Ener.* **36**, 10816 (2011).
- [248] X. Jiang, X. Cheng, G. Chen, and H. Zhang, *Int. J. Quantum Chem.* **112**, 2627 (2012).
- [249] T. N. Olney, N. M. Cann, G. Cooper, and C. E. Brion, *Chem. Phys.* **223**, 59 (1997).
- [250] K. Sumida, D. Stück, L. Mino, J.-D. Chai, E. D. Bloch, O. Zavorotynska, L. J. Murray, M. Dinca, S. Chavan, S. Bordiga, M. Head-Gordon, and J. R. Long, *J. Am. Chem. Soc.* **135**, 1083 (2013).
- [251] L. Kong, V. R. Cooper, N. Nijem, K. Li, J. Li, Y. J. Chabal, and D. C. Langreth, *Phys. Rev. B* **79**, 081407(R) (2009).
- [252] A. K. Mishra, S. Ramaprabhu, *AIP Advances* **1**, 032152 (2011).
- [253] S. C. Xu, S. Irle, D. G. Musaev, and M. C. Lin, *J. Phys. Chem. B* **110**, 21135 (2006).
- [254] D. Umadevi and G. N. Sastry, *J. Phys. Chem. C* **115**, 9656 (2011).
- [255] K.-J. Lee and S.-J. Kim, *Bull. Korean Chem. Soc.* **34**, 10 (2013).
- [256] D. Quiñonero, A. Frontera, P. M. Deyà, *J. Phys. Chem. C* **116**, 21083 (2012).
- [257] M. Bienfait, P. Zeppenfeld, N. Dupont-Pavlovsky, M. Muris, M. R. Johnson, T. Wilson, M. DePies, and O. E. Vilches, *Phys. Rev. B* **70**, 035410 (2004).
- [258] J. J. Zhao, A. Buldum, J. Han, and J. P. Lu, *Nanotechnology* **13**, 195 (2002).
- [259] D. G. A. Smith and K. Patkowski, *J. Phys. Chem. C* **118**, 544 (2014).
- [260] See www.auburn.edu/cosam/faculty/chemistry/patkowski/
- [261] P. Cabrera-Sanfelix, *J. Phys. Chem. A* **113**, 493 (2009).
- [262] Y. Liu and J. Wilcox, *Environ. Sci. Technol.* **45**, 809 (2011).
- [263] B. C. Wood, S. Y. Bhide, D. Dutta, V. S. Kandagal, A. D. Pathak, S. N. Punnathanam, K. G. Ayappa, and S. Narasimhan, *J. Chem. Phys.* **137**, 054702 (2012).
- [264] A. J. Du, C. H. Sun, Z. H. Zhu, G. Q. Lu, V. Rudolph, and S. C. Smith, *Nanotechnology* **20**, 375701 (2009).
- [265] C. Chen, K. Xu, X. Ji, L. Miao, and J. Jiang, *Phys. Chem. Chem. Phys.* **16**, 11031 (2014).
- [266] A. K. Mishra and S. Ramaprabhu, *J. Mater. Chem.* **21**, 7467 (2011).
- [267] S.-T. Yang, J. Kim, and W.-S. Ahn, *Micropor. and Mesopor. Mat.* **135**, 90 (2010).
- [268] Z. Yong, V. G. Mata, and A. E. Rodrigues, *Adsorption* **7**, 41 (2001).
- [269] B. Gao, J.-X. Zhao, Q.-H. Cai, X.-G. Wang, and X.-Z. Wang, *J. Phys. Chem. A* **115**, 9969 (2011).
- [270] Y. Jiao, Y. Zheng, S. C. Smith, A. Du, and Z. Zhu, *ChemSusChem* **7**, 435 (2014).
- [271] J.-J. Mo, Y. Xue, X.-Q. Liu, N.-X. Qiu, W. Chu, and H.-P. Xie, *Surface Science* **616**, 85 (2013).
- [272] C. Cazorla and S. A. Shevlin, *Dalton Trans.* **42**, 4670 (2013).
- [273] A. Franceschetti and A. Zunger, *Nature* **402**, 60 (1999).
- [274] S. V. Dudly and A. Zunger, *Phys. Rev. Lett.* **97**, 046401 (2006).
- [275] H. Ji, J. Park, M. Cho, and Y. Jung, *ChemPhysChem* **15**, 3157 (2014).
- [276] L. Valenzano, B. Civalieri, S. Chavan, G. T. Palomino, C. O. Areán, and S. Bordiga, *J. Phys. Chem. C* **114**, 11185 (2010).
- [277] R. Poloni, B. Smit, and J. B. Neaton, *J. Phys. Chem. A* **116**, 4957 (2012).
- [278] J. Park, H. Kim, S. S. Han, and Y. Jung, *J. Phys. Chem. Lett.* **3**, 826 (2012); J. Park, H. Kim, S. S. Han, and Y. Jung, *J. Phys. Chem. Lett.* **3**, 1582 (2012).
- [279] H. S. Koh, M. K. Rana, J. Hwang, and D. J. Siegel, *Phys. Chem. Chem. Phys.* **15**, 4573 (2013).
- [280] R. Poloni, K. Lee, R. F. Berger, B. Smit, and J. B. Neaton, *J. Phys. Chem. Lett.* **5**, 861 (2014).

- [281] K. D. Vogiatzis, A. Mavrandonakis, W. Klopper, and G. E. Froudakis, *ChemPhysChem* **10**, 374 (2009).
- [282] J. Witte, J. B. Neaton, and M. Head-Gordon, *J. Chem. Phys.* **140**, 104707 (2014).
- [283] M. K. Rana, H. S. Koh, J. Hwang, and D. J. Siegel, *J. Phys. Chem. C* **116**, 16957 (2012).
- [284] L. Valenzano, B. Civalleri, K. Sillar, and J. Sauer, *J. Phys. Chem. C* **115**, 21777 (2011).
- [285] S. Svelle, C. Tuma, X. Rozanska, T. Kerber, and J. Sauer, *J. Am. Chem. Soc.* **131**, 816 (2009).
- [286] S. Tosoni and J. Sauer, *J. Phys. Chem. Chem. Phys.* **12**, 14330 (2010).
- [287] M. Pozzo and D. Alfè, *Phys. Rev. B* **77**, 104103 (2008).
- [288] L. K. Wagner, *J. Phys.:Condens. Matt.* **19**, 343201 (2007).
- [289] D. Alfè and M. J. Gillan, *J. Phys.:Condens. Matt.* **18**, L435 (2006).
- [290] S. J. Binnie, E. Sola, D. Alfè and M. J. Gillan, *Molecular Simulation* **35**, 609 (2009).
- [291] L. K. Wagner and J. C. Grossman, *Phys. Rev. Lett.* **104**, 210201 (2010).
- [292] A. Badinski, P. D. Haynes, J. R. Trail, and R. J. Needs, *J. Phys.:Condens. Matt.* **22**, 074202 (2010).